A new 12 GeV proposal to Jefferson Lab PAC-34

The Δd Experiment:

Constraining d-Quark Polarization through Semi-Inclusive Spin Asymmetry Measurements on a Polarized ^{3}He Target

W. Chen, H. Gao, X. Qian, Y. Qiang, Q. Ye
Triangle Universities Nuclear Laboratory, Duke University, Durham, North Carolina.

P. Markowitz
Florida International University, Miami, Florida.

P. Bosted, J.-P. Chen (Co-Spokesperson), E. Chudakov, J. Gomez, O. Hansen, D.W. Higinbotham, C. W. de Jager, M. Jones, J. .J. LeRose, R. Michaels, S. Nanda, A. Saha,V. Sulkosky
Thomas Jefferson National Accelerator Facility, Newport News, Virginia.

B.T. Hu, Y.W. Zhang, Y. Zhang
Lanzhou University, Lanzhou, P.R. China.

K. Allada, C. Dutta, W. Korsch
University of Kentucky, Lexington, Kentucky.

L. Guo, X. Jiang (Co-Spokesperson)[a] , H. Liu, M.-X. Liu
Los Alamos National Laboratory, Los Alamos, New Mexico.

W. Bertozzi, S. Gilad, J. Huang
Massachusetts Institute of Technology, Cambridge, Massachusetts.

J. R. Calarco, K. Slifer
University of New Hampshire, Durham, New Hampshire.

D. Armstrong, T. Averett
College of William and Mary, Williamsburg, Virginia.

L. El Fassi, R. Gilman, G. Kumbartzki, R. Ransome, E. Schulte
Rutgers University, Piscataway, New Jersey.

D. Day, R. Lindgren, N. Liyanage, V. Nelyubin, B. Norum, M. Shabestari, K. Wang, X. Zheng
University of Virginia, Charlottesville, Virginia.

Y. Jiang, H. Lu, X. Yan, Y. Ye
University of Science and Technology of China, Hefei, P.R.China.

[a]Contact person. Email: jiang@jlab.org

S. Zhou, X. Li
China Institute of Atomic Energy, Beijing, P.R.China.

E. Cisbani, F. Cusanno, S. Frullani, F. Garibaldi, S. Marrone, G. Urciuoli, M. Iodice, R. De Leo, L .La Gamba
INFN Roma–I, INFN Roma–III, INFN Bari and University of Bari, Italy.

S. Širca
University of Ljubljana, Slovenia.

Seonho Choi
Seoul National University, Seoul, Korea

J.R.M. Annand, G. Rosner
University of Glasgow, Glasgow, Scotland, United Kingdom.

Abstract: We propose to measure the beam-target double-spin asymmetries in semi-inclusive deep-inelastic $\vec{n}(\vec{e},e'\pi^+)X$ and $\vec{n}(\vec{e},e'\pi^-)X$ reactions on a longitudinally polarized ^{3}He target (kaon as by-products) at $\langle Q^2\rangle = 4.0$ GeV^2 and $x = 0.110 \sim 0.461$. The high statistics data from this experiment will be used as inputs to global NLO QCD analysis to put strong constraints on quark helicity distributions, $\Delta d(x)$ since the neutron asymmetries are most sensitive to d-quark contribution, and indirectly constrain gluon polarization. Different from other SIDIS measurements like HERMES and COMPASS, this experiment uses two independent magnetic spectrometers. By flipping the magnetic polarity of the hadron spectrometer, identical phase spaces between π^+ and π^- reaction can be achieved such that the combined asymmetry $A_{1He}^{\pi^+-\pi^-}$ can be determined with high precision. In $A_{1He}^{\pi^+-\pi^-}$, which is a charge and flavor non-singlet combination, contributions from gluons as well as sea-quarks cancel exactly to all orders of QCD, thus allow a direct determination of $\Delta d_v - \frac{1}{4}\Delta u_v$, independent of fragmentation functions. When combined with the expected world data on polarized proton, to obtain $\Delta u_v - \Delta d_v$, this experiment will provide the opportunity to address the polarized sea asymmetry $\Delta\bar{u} - \Delta\bar{d}$. The standard BigBite spectrometer, in the same electron-detector configuration as in the Neutron Transversity experiment (E06-010), will be used to detect the scattered electrons at 25°. The left-HRS spectrometer, with its septum magnet at 6°, will be used to detect the leading hadrons in coincidence ($p_h = 4.3$ GeV/c, $z \approx 0.5$). Other than the 11 GeV beamline instruments, all apparatus needed for this experiment exist and have been operational. A total of 28 days of 11 GeV beam in Hall A is requested.

Contents

1 Introduction

The last decade has seen remarkable progress in the knowledge of the polarized parton distribution functions (pPDF) $\Delta q_f(x)$. The most precise and clearly interpreted data are from inclusive deep-inelastic lepton scattering (DIS) experiments at CERN and SLAC. However, the information available from inclusive DIS process has inherent limitations. As the cross sections are only sensitive to e_q^2, the quark charge square, an inclusive experiment probes quarks and anti-quarks on an equal footing, and it is only possible to determine combinations of $\Delta q + \Delta\bar{q}$, but never the valence $\Delta q_v = \Delta q - \Delta\bar{q}$ nor the sea $\Delta\bar{q}$ separately. Therefore it is not sensitive to the symmetry breaking in the sea sector. Through inclusive DIS measurements, only one particular flavor non-singlet can be directly inferred i.e. $\Delta q_3(x, Q^2) = \Delta u + \Delta\bar{u} - \Delta d - \Delta\bar{d}$. The additional assumption of $\mathrm{SU}(3)_f$ flavor symmetry allows the hyperon beta decay data to constrain the first moments of Δq. The well-cited result of this approach is that quark helicities seem to make a small net contribution to the nucleon spin, and the strange sea appears to be negatively polarized.

The sensitivity to each individual quark flavor is realized in semi-inclusive deep inelastic scattering (SIDIS) in which one of the leading hadrons in quark fragmentation is also detected. Since the leading hadrons from the current fragmentation carry information about the struck quark's flavor, detection of the leading hadron effectively "tags" the quark flavor. Therefore, SIDIS offers an unique opportunity for determining the spin, flavor, and sea structure of the nucleon [1], thereby significantly enriching our understanding of QCD and the nucleon structure. High precision polarized SIDIS data on the proton and the neutron (in a deuteron or a ^{3}He nuclei) allows a flavor decomposition of nucleon spin structure, which could lead to the discovery of a possible flavor-asymmetry in the polarized sea. In 2005, the HERMES collaboration published the results of a leading order spin flavor decomposition from polarized proton and deuteron data, and for the first time extracted the sea quark polarizations [2,3]. Unlike the predictions of several theoretical models, HERMES data indicated that within the available statistics $\Delta\bar{u} - \Delta\bar{d}$ is consistent with an unbroken $\mathrm{SU}(2)_f$ symmetry.

The HERMES data has demonstrated that, within the experimental precision, the semi-inclusive double-spin asymmetries A_{1N}^h at $\langle Q^2\rangle = 2.5$ GeV^2 agree reasonably well with the SMC data [4] at $\langle Q^2\rangle = 10$ GeV^2. very recently, COMPASS asymmetry data on deuteron [5], averaged at $\langle Q^2\rangle = 10$ GeV^2, was also shown to agree well with HERMES data. This non-trivial agreement indicates that semi-inclusive asymmetries have rather weak Q^2 dependencies and the expected violation of naive leading order x-z separation is not large. The apparent "precocious scaling" suggests that at a modest Q^2, such as at HERMES $\langle Q^2\rangle = 2.5$ GeV^2 and at $\langle Q^2\rangle = 4.0$ GeV^2 for this experiment, information on the quark distributions should be reasonably well-preserved in semi-inclusive reactions. Ji, Ma and Yuan have explicitly proved [6] that QCD factorization is valid for SIDIS with hadrons emitted in the current frag-

mentation region with low transverse momentum $p_{\perp h} \ll Q$. QCD factorization of spin-dependent cross sections in SIDIS and Drell-Yan has also been proved for the low $p_{\perp h}$ case [7]. JLab E00-108 data [8], on unpolarized SIDIS cross section ratios of proton and deuteron with 5.5 GeV beam and $\langle Q^2 \rangle = 2.3$ GeV^2, also indicated that the leading order naive x-z separation is rather close to the reality.

It was pointed out by Frankfurt et al. [1] and by Christova and Leader [9] that if the combined asymmetries $A_{1N}^{\pi^+-\pi^-}$ are measured with high enough precision, quark polarization Δu_v, Δd_v and $\Delta\bar{u} - \Delta\bar{d}$ can be extracted at leading order independent of the knowledge of fragmentation functions. Even at the next-to-leading order, information on the valence quark polarizations is well-preserved in the combined asymmetries $A_{1N}^{\pi^+-\pi^-}$, due to the fact that contributions from gluons as well as sea-quarks cancel exactly to all orders of QCD [9] in this charge and flavor non-singlet combination. In practice, the combined asymmetry $A_{1N}^{\pi^+-\pi^-}$ poses more experimental challenges, since precise knowledge on hadron phase spaces and detection efficiencies are required. This experiment is specifically designed to measure $A_{1N}^{\pi^+-\pi^-}$. Different from other SIDIS measurements like HERMES and COMPASS, this experiment will use two independent magnetic spectrometers. By flipping the magnetic polarity of the hadron spectrometer, identical phase spaces between π^+ and π^- reaction can be achieved such that the combined asymmetry $A_{1He}^{\pi^+-\pi^-}$ can be determined with high precision. At Q^2 of 2.0 $\sim$ 6.7 GeV^2, and $x = 0.110 \sim 0.461$, this experiment will provide independent precision data on $\Delta d_v - \frac{1}{4}\Delta u_v$. When combined with the expected world data on polarized proton, to obtain $\Delta u_v - \Delta d_v$, this experiment will provide the opportunity to address the polarized sea asymmetry $\Delta\bar{u} - \Delta\bar{d}$.

At the next-to-leading order, following the well established formalism [10], tools of NLO QCD global fits, which include data sets from both inclusive and semi-inclusive reactions, have become available [11]. Recently, such global NLO QCD fit has also included RHIC pp data [12]. Currently, the world data on SIDIS asymmetries only includes one ^{3}He data set, with rather large error bars, obtained by HERMES in 1996. The high statistics ^{3}He data from this experiment, adding much precise neutron SIDIS asymmetries to the world data sample, will serve as stringent constraints on pPDFs through NLO global fits [13]. Indirectly, the constraint on Δg coming from the addition of data from this experiment is as stringent as the $A_{LL}^{\pi^0}$ data from PHENIX experiment of RHIC run-2006 [13,14]. The main source of this sensitivity to Δg comes from the Q^2-evolutions of the inclusive g_1 structure function, but now with sea and valence contributions much better separated by semi-inclusive data in the global fit [11,13].

Jefferson Lab Hall A, with its high luminosity polarized ^{3}He target, has the unique advantage in providing high precision neutron asymmetry data in nucleon spin studies. Hall A data on inclusive A_{1n} and g_2^n measurements [15,16] has improved previous world knowledge by an order of magnitude in each case. The Hall A polarized ^{3}He target system has been under continuous improvements over the last decade. Recently, it reached an average in-beam polarization of 65% during the Neutron Transversity experiment (E06-010). A large acceptance magnetic spectrometer, the

BigBite spectrometer, with its electron detector package has been in operation currently in Neutron Transversity. At 11 GeV beam energy, SIDIS measurement can reach $\langle Q^2 \rangle = 4.0$ GeV^2 and $\langle W \rangle = 3.5$ GeV, at which point the direction of the momentum transfer $\vec{q}$ is as forward as 6°. To detect the leading hadron in the current fragmentation regime, the hadron spectrometer should be arranged to be directly along $\vec{q}$. The Hall A HRS spectrometer with its septum magnet provide such an access at small angle. Together, the combination of a high polarization electron beam at 11 GeV, a high luminosity and high polarization ^{3}He target, a large acceptance magnetic spectrometer, and the capability of small angle access of HRS+septum make it possible for a dramatic improvement on the world data set of SIDIS neutron asymmetries.

2 Physics Motivation

The principle goal of spin-dependent SIDIS experiments is to perform flavor decomposition of nucleon spin structure taking advantage of flavor tagging. In this section, we first express the SIDIS cross sections and asymmetries at leading order (LO) and summarize the HERMES results of "purity method" (more details in Appendix). After introducing the next-to-leading order cross sections, we summarize the NLO global QCD analysis method. We will then outline new methods of flavor decomposition: the Christova-Leader method at leading order and next-to-leading order. Theoretical models of polarized light sea asymmetry $\Delta\bar{u} - \Delta\bar{d}$ is summarized at the end. Throughout this proposal, SU(2) isospin symmetry and charge conjugation invariance are assumed and heavy quark contributions are neglected.

2.1 Beam-target double-spin asymmetries at leading order

At the leading order, the SIDIS process is separated into a hard-scale quark scattering followed by a soft-scale hadronization. The "naive x-z separation" assumption, on which the SMC and HERMES analysis were based, implies that the spin-independent (σ^h) and the spin-dependent ($\Delta\sigma^h$) cross sections follow:

$$\sigma^h(x,z) = \sum_f e_f^2 q_f(x) \cdot D_{q_f}^h(z), \quad \Delta\sigma^h(x,z) = \sum_f e_f^2 \Delta q_f(x) \cdot D_{q_f}^h(z), \tag{1}$$

where $x = Q^2/2M\nu$, $z = E_h/\nu$. The fragmentation functions $D_{q_f}^h(z)$ represent the probability that a quark f fragments into a hadron h.

Considering the beam and target polarization (P_B and P_T), and the dilution factor ($f^h = \sigma_{pol.N}^h/\sigma_{allN}^h$), which accounts for the unpolarized nucleons in the target, the double-spin asymmetry [3] for a longitudinally polarized beam on a longitudinally polarized target is :

$$A_\parallel^h = f^h P_B P_T \cdot \mathcal{P}_{kin} \cdot A_{1N}^h, \tag{2}$$

the kinematic factor $\mathcal{P}_{kin}$ is:

$$\mathcal{P}_{kin} = \mathcal{D} \cdot (1 + \gamma\eta) \cdot \frac{1+R}{1+\gamma^2}, \tag{3}$$

in which

$$\eta = \frac{2\gamma(1-y)}{2-y}, \qquad \mathcal{D} = \frac{1-(1-y)\epsilon}{1+\epsilon \cdot R},$$
$$\epsilon^{-1} = 1 + 2(1+\nu^2/Q^2)\tan^2(\theta_e/2), \tag{4}$$

$\mathcal{D}$ is the virtual photon polarization, $R(x,Q^2) = \sigma_L/\sigma_T$ accounts for the longitudinal component of the virtual photon and $y = \nu/E_0$, $\gamma^2(x,Q^2) = 4M^2x^2/Q^2$. In the current fragmentation regime, the virtual photon asymmetry is defined as:

$$A_{1N}^h(x,Q^2,z) \equiv \frac{\Delta\sigma^h(x,Q^2,z)}{\sigma^h(x,Q^2,z)} = \frac{\sum_f e_f^2 \Delta q_f(x,Q^2) \cdot D_{q_f}^h(z,Q^2)}{\sum_f e_f^2 q_f(x,Q^2) \cdot D_{q_f}^h(z,Q^2)}. \tag{5}$$

Each individual measurement on $A_{1N}^h(x,Q^2,z)$ provides an independent constrain on the polarized parton distributions $\Delta q_f(x,Q^2)$. Data from HERMES on proton and deuteron, and from COMPASS on deuteron target are summarized in Appendix-A.

In principle, the asymmetry A_{1N}^h depends on both variables x and z, its x-dependency comes from parton distributions and z-dependency comes from fragmentation functions. Generally speaking, accurate knowledge of the fragmentation functions is crucial in order to extract quark polarizations from the measured asymmetries according to Eq. 5. However, in some special combinations, if σ^h and $\Delta\sigma^h$ happen to have similar z-dependencies, as their ratio, the asymmetry will end up with a weak or even vanishing z-dependency. This type of cancellation can provide us with much cleaner observables to access quark polarizations without the complication of fragmentation functions. For example, Christova and Leader pointed out [9] that at the leading order, under the assumptions of SU(2) isospin symmetry and charge conjugation invariance, the fragmentation functions canceled exactly in the combined $h^+ \pm h^-$ double-spin asymmetries. Furthermore, if strange quark contribution can be neglected, the semi-inclusive asymmetry $A_{1N}^{\pi^+ + \pi^-}$ is reduced to the inclusive asymmetry A_{1N}. Indeed, at the next-to-leading order, the z-dependence of $A_{1N}^{\pi^+ \pm \pi^-}$ is predicted to be very small [11].

2.2 HERMES results from leading order purity method

The HERMES result of flavor decomposition [2] is shown in Fig. 1. As expected, u-quarks are strongly polarized in the direction of proton spin, while d-quarks are polarized opposite to the proton spin. The sea quark polarizations are consistent with zero. Fig. 1 right panel shows the HERMES result of $x(\Delta\bar{u} - \Delta\bar{d})$ together with predictions of a broken $\mathrm{SU}(2)_f$ symmetry [17,18]. The data are consistent with an unbroken $\mathrm{SU}(2)_f$ sea symmetry.

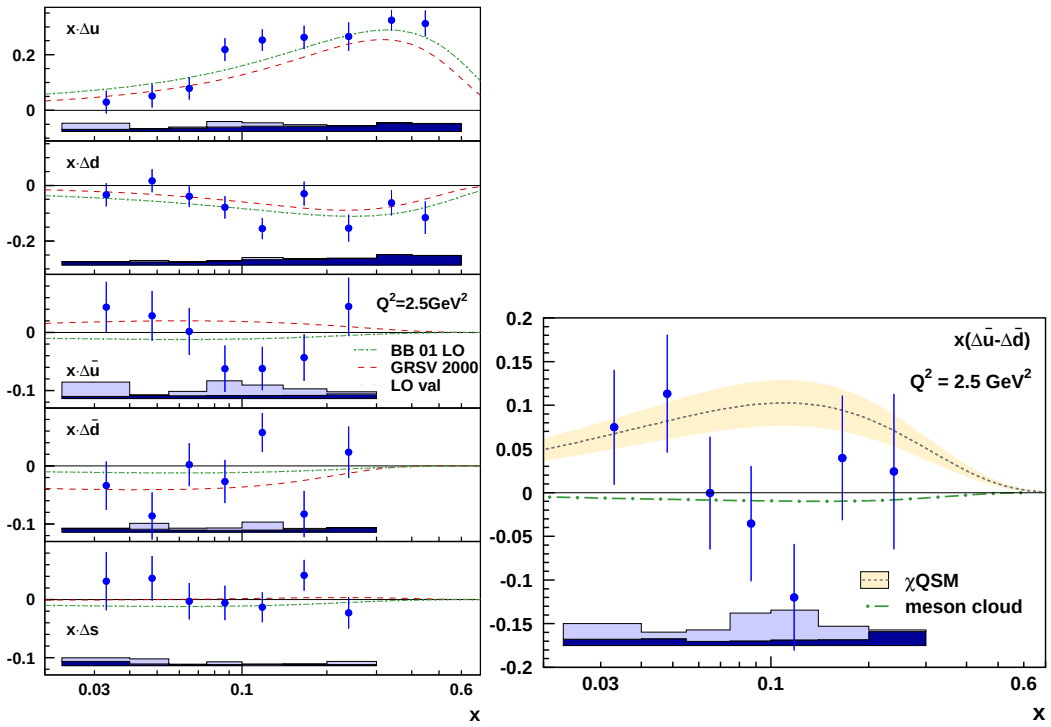

Figure 1: The HERMES result [2] of polarized quark distribution $x \cdot \Delta q(x)$ for u, $\bar{u}$, d, $\bar{d}$, and $s + \bar{s}$ versus x in comparison with two different parametrizations [19,20] is shown on the left. The difference of the polarized light sea $x(\Delta\bar{u} - \Delta\bar{d})$ is shown on the right. The error bars are statistical, while the shaded bands at the bottom indicate the systematic uncertainties.

The HERMES results left much room for improvement, with respect to statistical accuracies, especially on $\Delta\bar{u} - \Delta\bar{d}$. In addition, the validity and the stability of the leading order purity method needs to be independently verified. As pointed out by many authors, the issue of leading order violation of naive x-z separation and the intrinsic uncertainties of the fragmentation Monte Carlo simulation need to be quantitatively addressed at a level appropriate to the sea contribution [9].

2.3 Neutron SIDIS asymmetries are sensitive to Δd and $\Delta\bar{d}$

For a proton and a deuteron target, one expects u-quark dominates in SIDIS cross section due to e_q^2 weighting, as in the case of HERMES and COMPASS data. However, one expects Δd to be better constrained by neutron data from a polarized ^{3}He target. In Fig. 2, the fractional contribution of each quark flavor to the SIDIS cross sections σ_q^h/σ_{all} are shown for proton (left panel) and neutron (right panel), that is:

$$\frac{\sigma_q^h}{\sigma_{all}} = \frac{e_q^2 \cdot q(x,Q^2) \cdot D_q^h(z,Q^2)}{\sum_f e_f^2 \cdot q_f(x,Q^2) \cdot D_f^h(z,Q^2)}. \tag{6}$$

Sensitivities to d and $\bar{d}$ contributions in the neutron SIDIS cross sections are clearly demonstrated. The HERMES collaboration collected limited polarized ^{3}He data

back in 1996, which formed the basis of its first flavor decomposition paper [21].

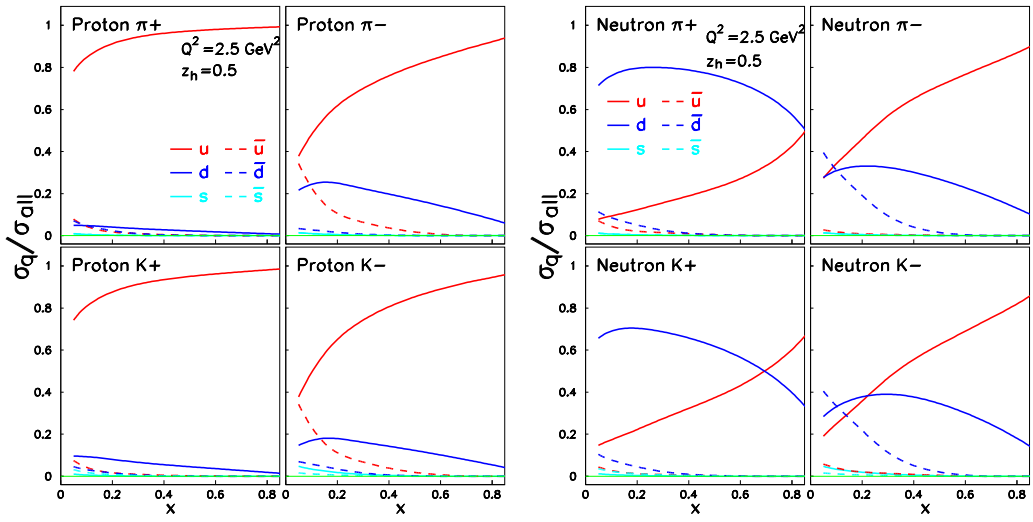

Figure 2: The left panel shows the proton SIDIS cross sections as fractional contributions from each quark flavor at $Q^2 = 2.5$ GeV^2 and $z = 0.5$. The right panel shows the case for a neutron.

2.4 SIDIS Cross sections at the next-to-leading order

The naive x-z separation is no longer valid at the next-to-leading order when gluon diagrams in Fig. 3 are considered. However, the exact form of the NLO cross section has been well-known [22]. At NLO, the terms of $q(x) \cdot D(z)$ and $\Delta q(x) \cdot D(z)$ in Eq. 1 are added with the double convolutions of the type $q \otimes \mathcal{C} \otimes D$ and $\Delta q \otimes \Delta C \otimes D$ in which $\mathcal{C}$ and ΔC are well-known Wilson coefficients [23]:

$$[q \otimes C \otimes D](x,z) = \int_x^1 \frac{dx'}{x'} \int_z^1 \frac{dz'}{z'} q\left(\frac{x}{x'}\right) C(x',z') D\left(\frac{z}{z'}\right). \tag{7}$$

We define the short-hand notation:

$$qD + \frac{\alpha_s}{2\pi} q \otimes C \otimes D = q\left[1 + \otimes \frac{\alpha_s}{2\pi} C \otimes\right] D, \tag{8}$$

at NLO instead of Eq. 1, we have:

$$\begin{aligned}
\sigma^h(x,z) &= \sum_f e_f^2 q_f \left[1 + \otimes \frac{\alpha_s}{2\pi} \mathcal{C}_{qq} \otimes\right] D_{q_f}^h \\
&+ \left(\sum_f e_f^2 q_f\right) \otimes \frac{\alpha_s}{2\pi} \mathcal{C}_{qg} \otimes D_G^h + G \otimes \frac{\alpha_s}{2\pi} \mathcal{C}_{gq} \otimes \left(\sum_f e_f^2 D_{q_f}^h\right), \qquad (9) \\
\Delta\sigma^h(x,z) &= \sum_f e_f^2 \Delta q_f \left[1 + \otimes \frac{\alpha_s}{2\pi} \Delta C_{qq} \otimes\right] D_{q_f}^h \\
&+ \left(\sum_f e_f^2 \Delta q_f\right) \otimes \frac{\alpha_s}{2\pi} \Delta C_{qg} \otimes D_G^h + \Delta G \otimes \frac{\alpha_s}{2\pi} \Delta C_{gq} \otimes \left(\sum_f e_f^2 D_{q_f}^h\right) \qquad (10)
\end{aligned}$$

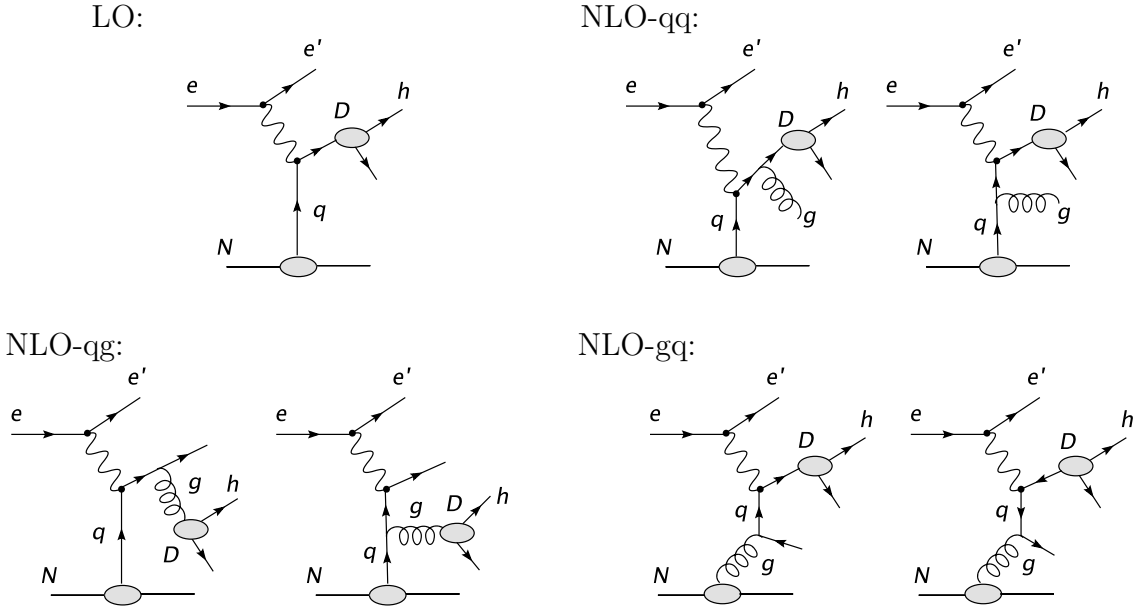

Figure 3: SIDIS diagrams at leading order (LO) and the next-to-leading order (NLO).

It is also well-known that in the Mellin-n space, the double-convolutions factorize into simple products under moments, and the parton distributions can be recovered by an inverse Mellin transformation with all moments of Wilson coefficients already calculated [24].

2.5 NLO global QCD analysis of DIS and SIDIS data

At the next-to-leading order, the cross sections in Eq. 5 are replaced by Eq. 9 and Eq. 10. Following the well established [10] formalism, tools of NLO QCD global fits, which include data sets from inclusive and semi-inclusive reactions as well as pp data, have become available [11,12], and the uncertainties of the pPDF can be addressed in the global fits. With the HERMES results, the polarized SIDIS data have a non-negligible weight in the combined global analysis, comparable to that of inclusive data. It helped to constrain the sea quark and gluon polarization complementing the information obtained from DIS. The NLO global fit [11] to the existing DIS and SIDIS data are shown in Fig. 29 in Appendix.

The precision data from this experiment, adding the neutron asymmetries to the world data, will serve as stringent constraints on pPDFs through NLO global fits [13]. The impacts on pPDF moments are presented in the result section. Since the combined asymmetries $A_{1n}^{\pi^+-\pi^-}$ are also measured in this experiment, the result of the NLO global fit can be cross checked with that from the NLO Christova-Leader method.

2.6 Method of spin-flavor decomposition

LO Christova-Leader method to obtain $\Delta u_v(x)$, $\Delta d_v(x)$ and $\Delta\bar{u}(x) - \Delta\bar{d}(x)$

At the leading order, under isospin symmetry and charge conjugation invariance, the fragmentation functions cancel exactly in the combined asymmetry $A_{1N}^{\pi^+\pm\pi^-}$. In addition, higher-twist terms in the fragmentation functions are also expected to be largely canceled [9]. In the quantities related to $\sigma^{\pi^+} - \sigma^{\pi^-}$ which is a charge and flavor non-singlet combination, sea-quarks and gluons do not contribute at any QCD-order [9].

From the Appendix, at leading order , for polarized protons, polarized deuterons and polarized neutrons [b] (in ^{3}He), we have:

$$A_{1p}^{\pi^+-\pi^-}(\vec{p}) = \frac{\Delta\sigma_p^{\pi^+} - \Delta\sigma_p^{\pi^-}}{\sigma_p^{\pi^+} - \sigma_p^{\pi^-}} = \frac{4\Delta u_v - \Delta d_v}{4u_v - d_v}, \tag{11}$$

$$A_{1d}^{\pi^+-\pi^-}(\vec{p}+\vec{n}) = \frac{\Delta\sigma_d^{\pi^+} - \Delta\sigma_d^{\pi^-}}{\sigma_d^{\pi^+} - \sigma_d^{\pi^-}} = \frac{\Delta u_v + \Delta d_v}{u_v + d_v}, \tag{12}$$

$$A_{1He}^{\pi^+-\pi^-}(\vec{n}+2p) = \frac{\Delta\sigma_{He}^{\pi^+} - \Delta\sigma_{He}^{\pi^-}}{\sigma_{He}^{\pi^+} - \sigma_{He}^{\pi^-}} = \frac{4\Delta d_v - \Delta u_v}{7u_v + 2d_v}. \tag{13}$$

Measurements on three different targets will over-determine Δu_v and Δd_v. Proton and deuteron measurements are more sensitive to Δu_v, measurements on ^{3}He are more sensitive to Δd_v. One can re-write the last relation as:

$$(\Delta d_v - \tfrac{1}{4}\Delta u_v)_{LO} = \frac{1}{4}\,(7u_v + 2d_v)\,A_{1He}^{\pi^+-\pi^-}. \tag{14}$$

This method of flavor decomposition involves helicity asymmetries of cross section differences. Kinematics need to be carefully chosen such that π^+ and π^- cross sections are reasonably different. Error propagation on $A_{1N}^{\pi^+-\pi^-}$ make this method unfavorable when π^-/π^+ ratio approaches unity. Fig. 27 in Appendix illustrates this point by comparing the purity method with the Christova-Leader method for HERMES data [3].

We can obtain the leading order quantity $\Delta u_v - \Delta d_v$ from combinations of either proton and ^{3}He data or proton and deuteron data as:

$$(\Delta u_v - \Delta d_v)_{LO} = \frac{1}{5}\left[\left(4u_v - d_v)A_{1p}^{\pi^+-\pi^-} - (7u_v + 2d_v)A_{1He}^{\pi^+-\pi^-}\right)\right], \tag{15}$$

$$(\Delta u_v - \Delta d_v)_{LO} = \frac{1}{5}\left[2\left(4u_v - d_v)A_{1p}^{\pi^+-\pi^-} - 3(u_v + d_v)A_{1d}^{\pi^+-\pi^-}\right)\right]. \tag{16}$$

On the other hand, constrained by the inclusive data, the flavor non-singlet quantity at all QCD orders is:

$$\Delta q_3(x, Q^2) \equiv (\Delta u + \Delta\bar{u}) - (\Delta d + \Delta\bar{d}). \tag{17}$$

[b] After the effective neutron polarization (86.5%) in ^{3}He is taken into account and the correction corresponding to the small proton polarization (2.8%) is applied.

The polarized sea asymmetry at all QCD orders is:

$$\Delta\bar{u} - \Delta\bar{d} = \frac{1}{2}\Delta q_3 - \frac{1}{2}(\Delta u_v - \Delta d_v). \tag{18}$$

At the leading order, we have:

$$\Delta q_3(x,Q^2)|_{LO} = 6\left[g_1^p(x,Q^2) - g_1^n(x,Q^2)\right], \tag{19}$$

$$\left[\Delta\bar{u}(x) - \Delta\bar{d}(x)\right]_{LO} = 3\left[g_1^p(x) - g_1^n(x))\right] - \frac{1}{2}(\Delta u_v - \Delta d_v)|_{LO}. \tag{20}$$

NLO Christova-Leader method

At the next-to-leading order, under isospin symmetry and charge conjugation invariance, the NLO convolution terms become much simpler in quantities that are related to $\sigma^{\pi^+} - \sigma^{\pi^-}$. Since the gluon-related terms are identical for π^+ and π^- production, they drop out in the differences [9]:

$$A_{1p}^{\pi^+-\pi^-}(\vec{p}) = \frac{(4\Delta u_v - \Delta d_v)\left[1 + \otimes(\alpha_s/2\pi)\Delta C_{qq}\otimes\right](D^+ - D^-)}{(4u_v - d_v)\left[1 + \otimes(\alpha_s/2\pi)\mathcal{C}_{qq}\otimes\right](D^+ - D^-)}, \tag{21}$$

$$A_{1d}^{\pi^+-\pi^-}(\vec{p}+\vec{n}) = \frac{(\Delta u_v + \Delta d_v)\left[1 + \otimes(\alpha_s/2\pi)\Delta C_{qq}\otimes\right](D^+ - D^-)}{(u_v + d_v)\left[1 + \otimes(\alpha_s/2\pi)\mathcal{C}_{qq}\otimes\right](D^+ - D^-)}, \tag{22}$$

$$A_{1He}^{\pi^+-\pi^-}(\vec{n}+2p) = \frac{(4\Delta d_v - \Delta u_v)\left[1 + \otimes(\alpha_s/2\pi)\Delta C_{qq}\otimes\right](D^+ - D^-)}{(7u_v + 2d_v)\left[1 + \otimes(\alpha_s/2\pi)\mathcal{C}_{qq}\otimes\right](D^+ - D^-)}. \tag{23}$$

in which Δu_v and Δd_v evolve as non-singlets and do not mix with sea-quark and gluon densities. Therefore, measurements of $A_{1N}^{\pi^+-\pi^-}$ can determine Δu_v and Δd_v at the next-to-leading order without any consideration of gluon and sea distributions. The double-convolution terms in Eq. 21 are expected to introduce negligible z-dependency in $A_{1N}^{\pi^+-\pi^-}$ at the kinematics of this experiment, as demonstrated in calculation of de Florian, Navarro and Sassot [11].

The first moment of $\Delta u_v - \Delta d_v$ is related to the moment of $\Delta\bar{u} - \Delta\bar{d}$ through the Bjorken sum rule at all orders of QCD [25]. The Bjorken sum rule, written in terms of the moment $\Delta_1 q = \int_0^1 dx \Delta q$,

$$\begin{aligned}\Delta_1 q_3 &\equiv \left[\Delta_1 u(Q^2) + \Delta_1\bar{u}(Q^2)\right] - \left[\Delta_1 d(Q^2) + \Delta_1\bar{d}(Q^2)\right] \\ &= \left|\frac{g_A}{g_v}\right| = 1.2670 \pm 0.0035 \;\; \textit{valid in all QCD orders.}\end{aligned} \tag{24}$$

Therefore, valid in all QCD orders, we have:

$$\int_0^1 (\Delta\bar{u} - \Delta\bar{d})dx = \frac{1}{2}\left|\frac{g_A}{g_v}\right| - \frac{1}{2}\int_0^1 (\Delta u_v - \Delta d_v)dx. \tag{25}$$

In other words, if one measures the valence quark moment $\Delta u_v - \Delta d_v$ precise enough, for example to $\delta\left[\Delta_1 u_v - \Delta_1 d_v\right] = \pm 0.05$, one cam pin down the polarized sea asymmetry, to $\delta\left[\Delta_1 \bar{u} - \Delta_1 \bar{d}\right] = \pm 0.025$, that's eight standard deviations from the prediction of Chiral Quark Soliton model.

A well-defined procedure has been given [25] to obtain the moment $\Delta_1 u_v - \Delta_1 d_v$ directly from the measured asymmetries $A_{1N}^{\pi^+ - \pi^-}$ without first solving Eq. 21 point-to-point. The stability of this procedure has been demonstrated [25] using the HERMES-1999 data.

From the deuteron data alone, one can also form Γ_v, the first moment of $\Delta u_v + \Delta d_v$, and extract at leading order the moment:

$$\int_0^1 (\Delta \bar{u} + \Delta \bar{d}) dx = 3\Gamma_1^N - \frac{1}{2}\Gamma_v + \frac{1}{12} a_8 \tag{26}$$

where Γ_1^N is the moment of$g_1^N = (g_1^p + g_1^n)/2$ from inclusive data, and $a_8 = 3F - D$ is from hyperon β-decays.

The recent COMPASS results [5] of $A_d^{h^+ - h^-}$ are shown in Fig. 4. The extracted valence quark polarization $x(\Delta u_v + \Delta d_v)$ and the running-x_{min} integral of $\Delta u_v + \Delta d_v$ are shown in Fig. 5. The fact that the integral of $\Delta u_v + \Delta d_v$ is significantly different from that of assumption of a symmetrical polarized sea indicated that the sign of $\Delta \bar{u}$ is opposite to that of $\Delta \bar{d}$.

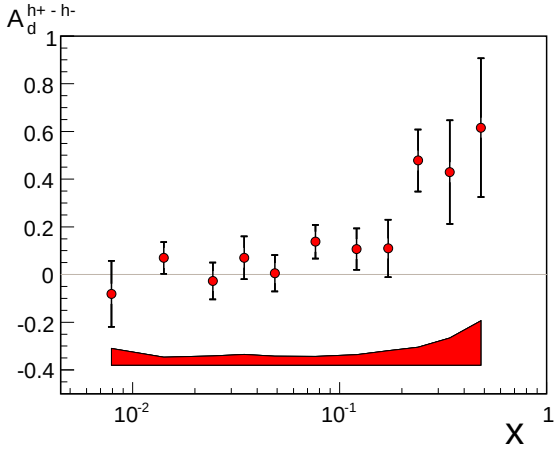

Figure 4: Charged hadron combined asymmetry $A_d^{h^+ - h^-}$ measured by COMPASS [5].

Cross check Δq_v with the upgraded RHIC

With the planned RHIC luminosity upgrade, Δq can be measured through $W^\pm$ decays [14]. Since the Q^2-evolutions of valence densities Δq_v are well understood in QCD, consistency cross checks can be made between JLab data at $\langle Q^2 \rangle = 4.0$ GeV^2 and RHIC data at $Q^2 = M_W^2$.

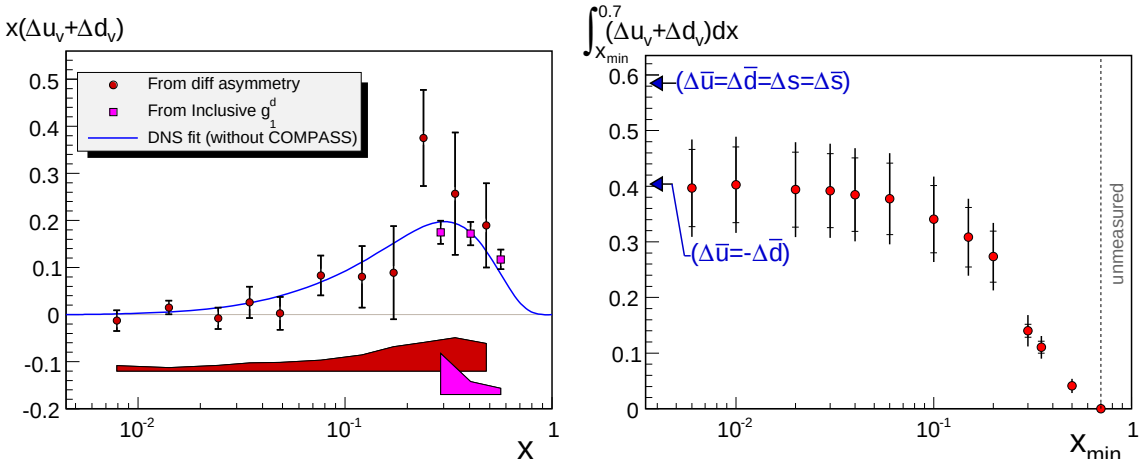

Figure 5: The valence quark polarization $x(\Delta u_v + \Delta d_v)$ compared with fron that of inclusive g_1^d data, and the running-x_{min} integral of $\Delta u_v + \Delta d_v$ from the deuteron data of COMPASS [5] at $Q^2 = 10$ GeV^2.

Spin observables to check the leading order naive x-z separation

A schematic strategy of to test leading order naive x-z separation was suggested [9] which requires prior knowledge of neither fragmentation functions nor parton distributions. The experimental observables in this strategy is to make the combined double-spin asymmetry $A_{1N}^{\pi^+ + \pi^-}$. If leading order naive x-z separation holds perfectly, $A_{1N}^{\pi^+ + \pi^-}$ will turn out to be identical to the inclusive A_{1N} asymmetry due to the exact cancellation of the fragmentation functions in the asymmetry under charge conjugation invariance and isospin symmetry. Their difference, $A_{1N}^{\pi^+ + \pi^-} - A_{1N}$, gives a clear indication on the size of the next-to-leading-order terms which violate the naive leading order x-z separation.

Assume $\Delta s = \Delta \bar{s} \approx 0$, the fragmentation functions are canceled at the leading order in the combined asymmetry $A_{1N}^{\pi^+ + \pi^-}$, such that:

$$A_{1p}^{\pi^+ + \pi^-}(x, Q^2, z) = \frac{\Delta\sigma_p^{\pi^+} + \Delta\sigma_p^{\pi^-}}{\sigma_p^{\pi^+} + \sigma_p^{\pi^-}} = \frac{4(\Delta u + \Delta\bar{u}) + \Delta d + \Delta\bar{d}}{4(u + \bar{u}) + d + \bar{d}} \equiv A_{1p}(x, Q^2),$$

$$A_{1d}^{\pi^+ + \pi^-}(x, Q^2, z) = \frac{\Delta\sigma_d^{\pi^+} + \Delta\sigma_d^{\pi^-}}{\sigma_d^{\pi^+} + \sigma_d^{\pi^-}} = \frac{\Delta u + \Delta d + \Delta\bar{u} + \Delta\bar{d}}{u + d + \bar{u} + \bar{d}} \equiv A_{1d}(x, Q^2),$$

$$A_{1n}^{\pi^+ + \pi^-}(x, Q^2, z) = \frac{\Delta\sigma_n^{\pi^+} + \Delta\sigma_n^{\pi^-}}{\sigma_n^{\pi^+} + \sigma_n^{\pi^-}} = \frac{\Delta u + \Delta\bar{u} + 4(\Delta d + \Delta\bar{d})}{u + \bar{u} + 4(d + \bar{d})} \equiv A_{1n}(x, Q^2) \quad (27)$$

The combined asymmetry $A_{1N}^{\pi^+ + \pi^-}$ reduces to the inclusive asymmetry A_{1N} under the leading order naive x-z separation. The relation $A_{1N}^{\pi^+ + \pi^-}(x, Q^2, z) = A_1(x, Q^2)$ is a rather strong condition to satisfy, since the left-hand side involves the hadron observable z while the right-hand side doesn't. The deviation of $A_{1N}^{\pi^+ + \pi^-}$ from the

inclusive A_{1N} asymmetry "effectively" measures the relative importance of the contribution from the next-to-leading order terms.

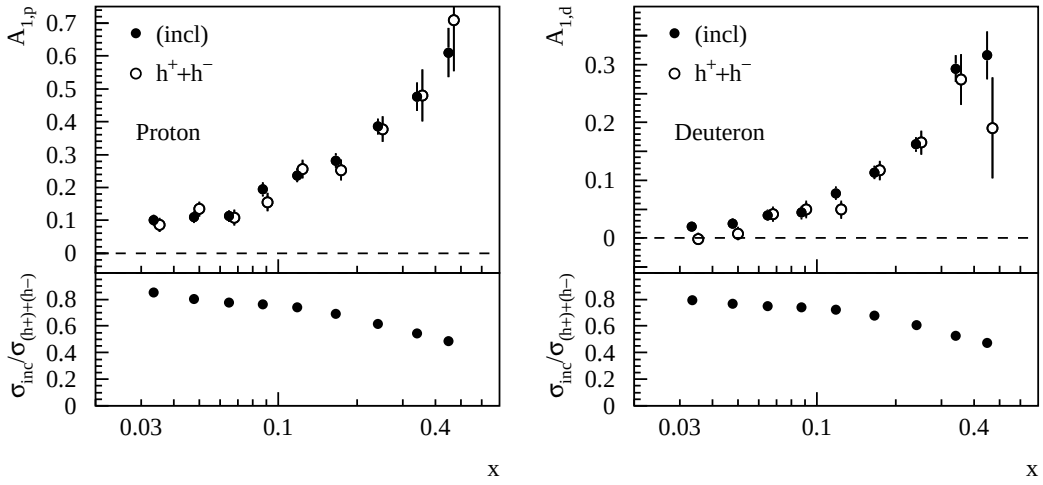

Figure 6: The HERMES inclusive asymmetries on the proton and the deuteron are compared with the respective semi−inclusive combined $h^+ + h^-$ asymmetries. The top panels show the asymmetries, where the hadron tagged asymmetry is offset in x for presentation. The lower panel shows the ratio of the uncertainties, $\delta(A_1)/\delta(A_{1N}^{h^+ + h^-})$.

The HERMES experiment extracted the combined asymmetry $A_{1N}^{h+\bar{h}}$ as shown in Fig. 6 in comparison with the inclusive asymmetry A_{1N}. The near perfect agreement of $A_{1N}^{h+\bar{h}}$ with A_{1N} at $\langle Q^2 \rangle = 2.5$ GeV^2 indicated that the next-to-leading order correction terms are small or mostly canceled in the asymmetries and the target fragmentation contribution has a negligible impact to the asymmetries. Even better agreements should be expected in this experiment at JLab-12GeV, since the much higher luminosity allow reasonable statistics at larger scattering angle resulted in $\langle Q^2 \rangle = 4.0$ GeV^2 for this experiment. Once this agreement can be clearly demonstrated with high precision, parton polarizations can be reliably extracted through the leading order interpretation of SIDIS asymmetries.

2.7 $\Delta\bar{u} - \Delta\bar{d}$: the flavor asymmetry in the polarized sea

Fermilab experiment E866 reported measurements of the yield ratio of Drell-Yan muon pairs from an 800 GeV/c proton beam incident on hydrogen and deuterium[26,27]. The data suggested a significantly asymmetric light sea quark distribution over an appreciable range in x; the asymmetry $\bar{d}/\bar{u}$ peaked around $x = 0.18$, as shown in Fig. 7. Furthermore, based on the E866 data and the CTEQ4M global-fit values of $\bar{u}+\bar{d}$, the values of $\bar{d}(x)-\bar{u}(x)$ were extracted, wit the moment $\int_0^1 \left[\bar{d}(x) - \bar{u}(x)\right] dx = 0.118 \pm 0.012$. Many theoretical models, including the meson cloud model, the chiral-quark model, the Pauli-blocking model, the instanton model, the chiral-quark soliton model and the statistical model, have been proposed to explain the $\bar{d}/\bar{u}$ asymmetry. These models can describe the $\bar{d} - \bar{u}$ reasonably well. However, they all have difficulties explaining the $\bar{d}/\bar{u}$ ratio at $x > 0.2$.

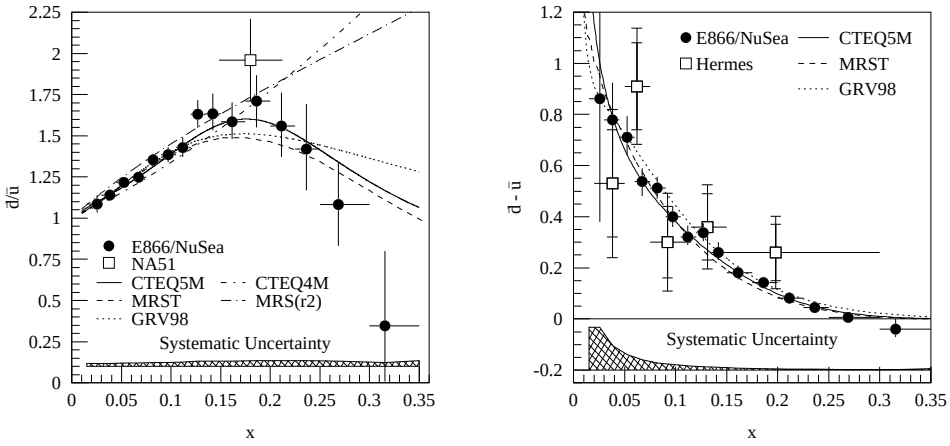

Figure 7: The Fermilab E866 results[26,27]. The left plot shows the ratio $\bar{d}/\bar{u}$ as a function of x, the right plot shows the extracted value of $\bar{d}(x) - \bar{u}(x)$ together with the HERMES semi-inclusive DIS results.

Since the unpolarized sea demonstrates a significant flavor asymmetry, one naively speculates a sizable flavor asymmetry also exists for the polarized sea in the same x-region. Indeed, many theory models have specific implications for the spin structure of the nucleon sea. For example, the Pauli-blocking model and the instanton model both predict a large asymmetry, $\int_0^1[\Delta\bar{u}(x) - \Delta\bar{d}(x)]dx = \frac{5}{3} \cdot \int_0^1[\bar{d}(x) - \bar{u}(x)]dx \approx 0.2$. In the chiral-quark soliton model, $\Delta\bar{u} - \Delta\bar{d}$ appears in leading-order (N_c^2) in a large N_c-expansion, while $\bar{d} - \bar{u}$ appears in the next-to-leading order (N_c). On the other hand, those meson cloud models which only include the π-meson predict $\Delta\bar{u} = \Delta\bar{d} = 0$ since the sea-quarks reside in a spin-0 π-meson. By considering a vector meson (ρ) cloud, non-zero sea polarization was predicted. A summary of theoretical predictions [28] of $I_\Delta = \int_0^1[\Delta\bar{u}(x) - \Delta\bar{d}(x)]dx$ are given in Table. 1. If the flavor asymmetry of the polarized sea is indeed as large as the predictions of many models shown in Table. 1, it would imply that a significant fraction of the Bjorken sum, $\int_0^1[g_1^p(x) - g_1^n(x)]dx$, comes from the flavor asymmetry of the polarized nucleon sea. The high statistics ^{3}He data from this experiment, together with the expected world proton data, will provide us with the first opportunity to discover the asymmetry in the polarized sea.

3 The Proposed Measurement

3.1 Overview

We plan to study the $\vec{n}(\vec{e}, e'h)X$ reactions ($h = \pi^+$ and π^-. K^+ and K^- as by-products) with a longitudinally polarized ^{3}He target in Hall A with a 11 GeV polarized electron beam. Relative yields will be determined for $(e, e'\pi^+)$ and $(e, e'\pi^-)$ reactions such that the combined asymmetries $A_{1N}^{\pi^+ \pm \pi^-}$ can be constructed in addition to the various double-spin asymmetries A_{1n}^h. As shown in Fig. 8, the left-HRS

Model	I_Δ prediction	Authors and References
Meson cloud (π-meson)	0	Eichten *et al.*[29], Thomas[30]
Meson cloud (ρ-meson)	$\simeq -0.007$ to -0.027	Fries *et al.*[31]
Meson cloud ($\pi-\rho$ interference)	$= -6\int_0^1 g_1^p(x)dx \simeq -0.7$	Boreskov *et al.*[32]
Meson cloud (ρ and $\pi-\rho$ interference)	$\simeq -0.004$ to -0.033	Cao *et al.*[18]
Meson cloud (ρ-meson)	< 0	Kumano *et al.*[33]
Meson cloud ($\pi-\sigma$ interference)	$\simeq 0.12$	Fries *et al.*[34]
Pauli-blocking (bag model)	$\simeq 0.09$	Cao *et al.*[18]
Pauli-blocking (ansatz)	$\simeq 0.3$	Gluck *et al.*[35]
Pauli-blocking	$= \frac{5}{3}\int_0^1[\bar{d}(x)-\bar{u}(x)]dx \simeq 0.2$	Steffens[36]
Chiral-quark soliton	0.31	Dressler[37]
Chiral-quark soliton	$\simeq \int_0^1 2x^0.12[\bar{d}(x)-\bar{u}(x)]dx$	Wakamatsu *et al.*[38]
Instanton	$= \frac{5}{3}\int_0^1[\bar{d}(x)-\bar{u}(x)]dx \simeq 0.2$	Dorokhov[39]
Statistical	$\simeq \int_0^1[\bar{d}(x)-\bar{u}(x)]dx \simeq 0.12$	Bourrely *et al.*[40]
Statistical	$> \int_0^1[\bar{d}(x)-\bar{u}(x)]dx \simeq 0.12$	Bhalerao[41]

Table 1: A summary[28] of theoretical predictions of $I_\Delta = \int_0^1[\Delta\bar{u}(x) - \Delta\bar{d}(x)]dx$.

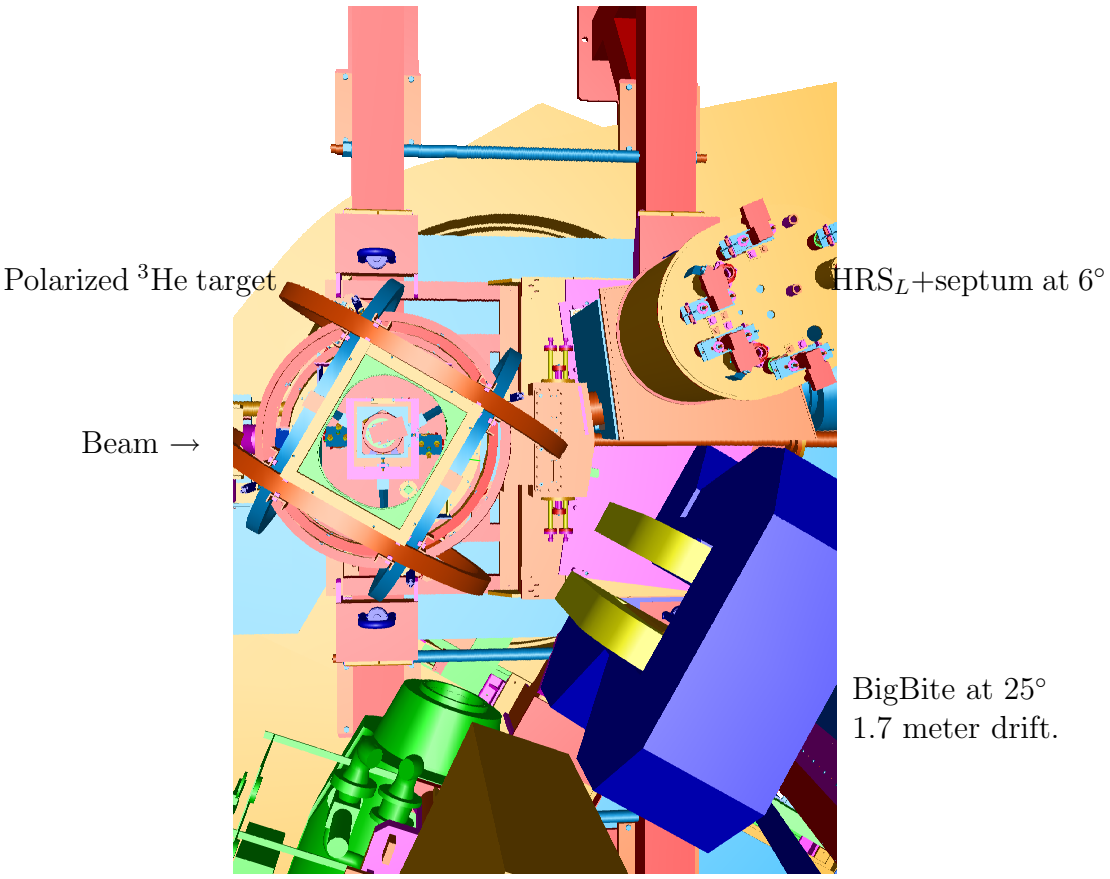

Figure 8: A top view illustration of the Hall A instruments near the interaction points for this experiment. Beam comes in from the left side. Left septum coupled with HRS is at 6°, the BigBite spectrometer is shown on beam right at 25° with a drift distance of 1.7 meter. The right HRS is parked at 110°, not in use.

spectrometer with its septum magnet will be located at 6° as the hadron detector at a central momentum of 4.30 GeV/c in either positive or negative polarity. For the electron arm the BigBite spectrometer, with its standard electron-detector package in the same configuration as in the neutron transversity experiment [42] (E06-010) , will be used to detect $(e, e'h)$ events in coincidence.

3.2 Kinematics and phase space

The definitions of the kinematics variables are the following: Bjorken-x, which indicates the fractional momentum carried by the struck quark, $x = Q^2/(2\nu M_N)$, M_N is the nucleon mass. The momentum of the outgoing hadron is p_h and the fraction of the virtual photon energy carried by the hadron is: $z = E_h/\nu$. W is the invariant mass of the whole hadronic system and W' is the invariant mass of the hadronic

system without the detected hadron. We have:

$$W^2 = M_N^2 + Q^2(\frac{1}{x} - 1),$$
$$W'^2 = (M_N + \nu - E_\pi)^2 - |\vec{q} - \vec{p}_\pi|^2. \quad (28)$$

We have chosen to cover the highest possible W with a 11 GeV beam, $2.95 < W < 4.19$ GeV, corresponds to $0.110 < x < 0.461$ and $2.06 < Q^2 < 6.70$ (GeV/c)^2. We chose to detect the leading hadron which carries $z \approx 0.5$ of the energy transfer to strongly favor the current fragmentation regime. The value of missing mass W' is chosen to be as high as possible (2.03∼3.19 GeV) to avoid contributions from resonance structures. The nominal kinematic values for each x-bin are listed in Table 2.

E′ GeV	θ_e deg.	x	W GeV	Q^2 GeV^2	θ_q deg.	z_π	p_h GeV/c	W'_π GeV	η^π_{cm}	x^π_F
						$\theta_h = 6.0°$				
1.00	25.0	0.110	4.19	2.06	2.4	0.43	4.30	3.19	1.78	0.42
1.75	25.0	0.208	3.84	3.61	4.5	0.47	4.30	2.86	2.29	0.46
2.50	25.0	0.323	3.42	5.15	6.9	0.51	4.30	2.48	2.41	0.51
3.25	25.0	0.461	2.95	6.70	9.7	0.56	4.30	2.03	1.67	0.54

Table 2: The nominal kinematics for the central BigBite angle of 25° and HRS angle of 6.0°. The HRS momentum setting ($p_{HRS} = 4.30$ GeV/c) and the central z and W' values are listed. Data of all x-bins will be collected simultaneously. Higher x-bins ($x > 0.461$) are not listed.

The phase space coverage is obtained from a detailed Monte Carlo simulation which includes realistic septum and HRS spectrometer models, detector geometry and target geometry. The HRS spectrometer with its septum magnet has a nominal solid angle of 5.0 msr and a momentum bite of ±4.5%. The BigBite spectrometer at 1.7 meter drift distance has an effective solid angle of 50 msr. The phase space covered in this experiment is shown in Fig. 9 for (x, E'), (x, W) and $x(, Q^2)$. We have $\langle Q^2 \rangle = 4$ GeV^2. By setting the hadron arm at 6°, directly along the average $\vec{q}$ direction, we cover the azimuthal angle as unbiased as possible. Hadron transverse momentum coverage is $0 < P_{h\perp} < 0.5$ GeV/c. Hadron azimuthal angle ($\phi_{\pi q}$) and polar angle ($\theta_{\pi q}$) coverage relative to the $\vec{q}$ direction is shown in Fig. 10.

Fig. 11 illustrates the phase space of η^π_{cm} vs x^π_F in this experiment, where the center-of-mass rapidity $\eta_{CM} = \frac{1}{2} ln \frac{E+P^\star_L}{E-P^\star_L}$ is defined in the center-of-mass frame. The separation in center-of-mass rapidity η^π_{cm} in this experiment is comparable to the regularly used Berger's criterion of $\Delta\eta_{CM} \geq 4.0$ for separation of current and target fragmentation [43].

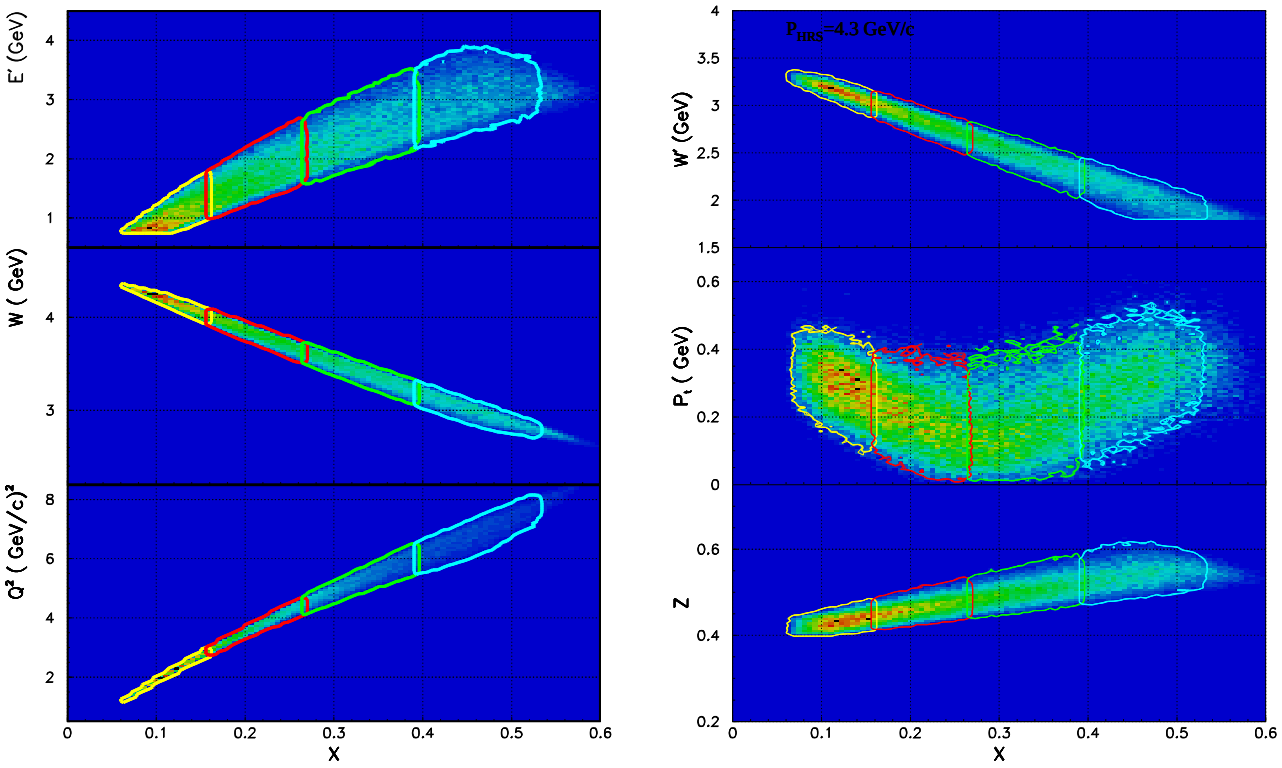

Figure 9: Left panel: the phase space coverage in (Q^2, x) and (W, x) planes for each x-bin. Phase space beyond $E' = 4.0$ GeV is not plotted. Right panel: phase space coverage in (W', x), (p_t, x) and (z, x) planes. The actual kinematic coverage is wider compared with the nominal values listed in Table 2.

3.3 The experimental observables

The beam and target double-spin asymmetries can be obtained directly from the number of events (N^+ and N^-) observed corresponding to each beam helicity, corrected by the luminosity ratio $\mathcal{L}^+/\mathcal{L}^-$:

$$A^h_{1He} = \frac{1}{f^h P_B P_T \mathcal{P}_{kin}} \cdot \frac{N^+ - N^- \cdot \dfrac{\mathcal{L}^+}{\mathcal{L}^-}}{N^+ + N^- \cdot \dfrac{\mathcal{L}^+}{\mathcal{L}^-}} \tag{29}$$

Since the CEBAF electron beam flips its helicity at a rate of 30 Hz, and a beam charge feed back system continuously controls the beam charge asymmetry Q^+/Q^- to below 100 ppm, practically, we have $\mathcal{L}^+/\mathcal{L}^- = 1$ for this experiment. The dilution factors f^h will be measured by comparing spectra from polarized target with that of the reference cell with Hydrogen, Helium-3 and Nitrogen gas. These dilution factors are expected to be measured to $\delta f/f \leq 2\%$ within a relatively short time. The uncertainties on the double-spin asymmetries δA^h_{1He} is dominated by the statistical uncertainties of $\delta A^h_{\parallel}$ with the dilution factor uncertainties play a minor role.

The combined asymmetry $A^{\pi^+\pm\pi^-}_{1He}$ needs the cross section ratio $r = \sigma^{\pi^-}_{He}/\sigma^{\pi^+}_{He}$ as

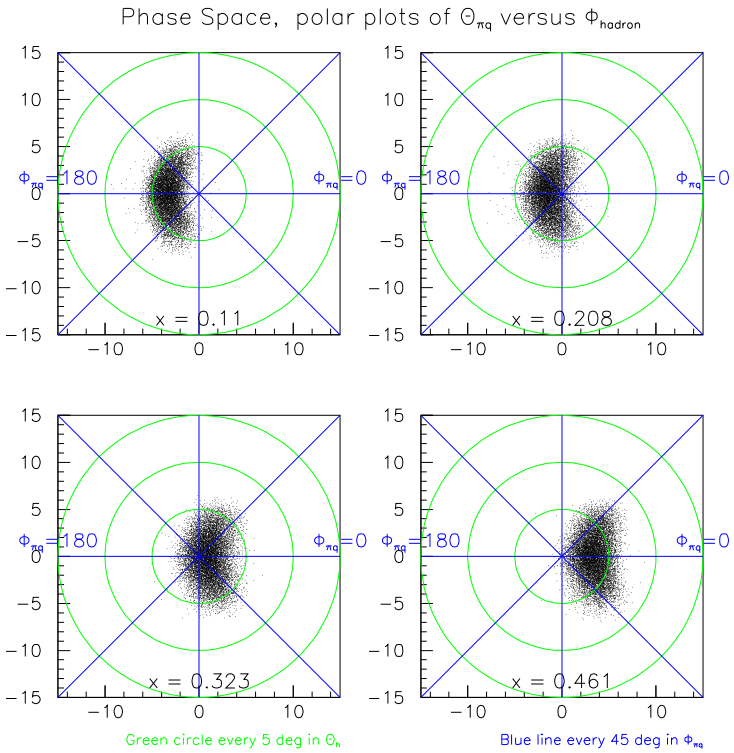

Figure 10: The hadron azimuthal angle ($\phi_{\pi q}$) and polar angle ($\theta_{\pi q}$) coverage for each x-bin. The $\vec{q}$ vector goes into the page at the middle of each plot.

an extra input:

$$A_{1He}^{\pi^+\pm\pi^-} = \frac{\Delta\sigma_{He}^{\pi^+} \pm \Delta\sigma_{He}^{\pi^-}}{\sigma_{He}^{\pi^+} \pm \sigma_{He}^{\pi^-}} = \frac{A_{1He}^{\pi^+} \pm A_{1He}^{\pi^-} \cdot r}{1 \pm r}. \tag{30}$$

For this experiment, we have roughly $r = \sigma_{He}^{\pi^-}/\sigma_{He}^{\pi^+} = 0.5 \sim 0.7$. The error propagation follows:

$$(\delta A_{1He}^{\pi^+\pm\pi^-})^2 = \frac{1}{(1 \pm r)^2}\left[(\delta A_{1He}^{\pi^+})^2 + r^2(\delta A_{1He}^{\pi^-})^2 + (A_{1He}^{\pi^-})^2(\delta r)^2 + (A_{1He}^{\pi^+\pm\pi^-})^2(\delta r)^2\right]. \tag{31}$$

The value of r can be easily determined to $|\delta r|/r \leq 2.0\%$ in this experiment since phase spaces are identical for π^+ and π^- measurements.

3.4 The electron arm: BigBite spectrometer

The BigBite spectrometer will be located at 25° and at a drift distance of 1.70 meter, instead of at 30° and 1.5 meter drift distance as in the Neutron Transversity experiment[42] (E06-010). At 1.7 m drift, the BigBite spectrometer has a solid angle of 50 msr, with a vertical acceptance of $\Delta\theta_t = \pm 210$ mrad and a horizontal acceptance of $\Delta\phi_t = \pm 60$ mrad. The BigBite dipole magnet will be set at the full current with

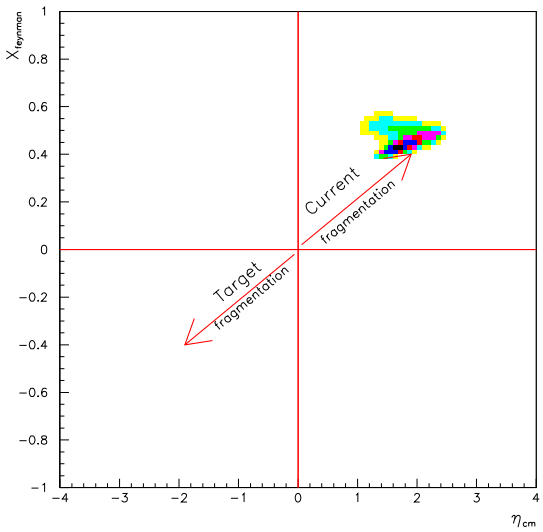

Figure 11: The center-of-mass rapidity η^{π}_{cm} vs x^{π}_{F}. For this experiment, the current and target fragmentation regime is separated by a rapidity gap of $\Delta\eta_{CM} \approx 4.0$.

$|\vec{B}| = 1.2$ T, in negative polarity. Through the dipole magnet, a typical charged particle of 1.4 GeV/c momentum is deflected by $\sim 10^{\circ}$.

As shown in Fig. 12, the BigBite detector package will be in the same configuration as in E06-010. Three wire chambers provide tracking information followed by a pre-shower, scintillator and shower assembly to provide trigger and particle ID for electrons. Although not critical for a coincidence measurement like in this proposal, a threshold gas Cherenkov detector will remain in place between the wire chambers to provide extra pion rejections in single-arm trigger such that inclusive A_{1n} measurements can be a possible by-product.

The pre-shower blocks are made of TF-5 lead glass, $10 \times 10 \times 37$ cm^3 each, covering an active area of 210×74 cm^2, with 10 cm (3 r.l.) along the particle's direction. The total absorption shower blocks are made of TF-2 lead glass, $8.5 \times 8.5 \times 34$ cm^3 each, covering an active area of 221×85 cm^2, with 34 cm (13 r.l.) along the particle's direction. The total depth of lead glass is enough to contain electron showers with energies up to 10 GeV. Trigger threshold will be set corresponding to 0.15 GeV in pre-shower and 0.50 GeV in total energy deposit, preventing the majority of pions from producing a trigger. The expected singles π^-/e^- ratio is $\sim$60:1 in this experiment.

The optics property of the BigBite spectrometer has been well studied at 1.1 m drift and 1.5 m drift. Typical track reconstruction qualities are shown in Fig. 13 left panel for vertex resolution δz_{tar} on multi-carbon foil targets along the beam direction, in Fig. 13 right panel for momentum resolution $\delta p/p$ in a $p(e,e')$ elastic calibration run. Typical momentum resolution is 1-2% for 1-2 GeV/c and 2-3% for 2-4 GeV/c. Fig. 14 shows the reconstructed track positions at the front of a 1.5 inch thick lead "slot slit" during a calibration run. The three small holes at the center each has an angular size of 11 mrad.

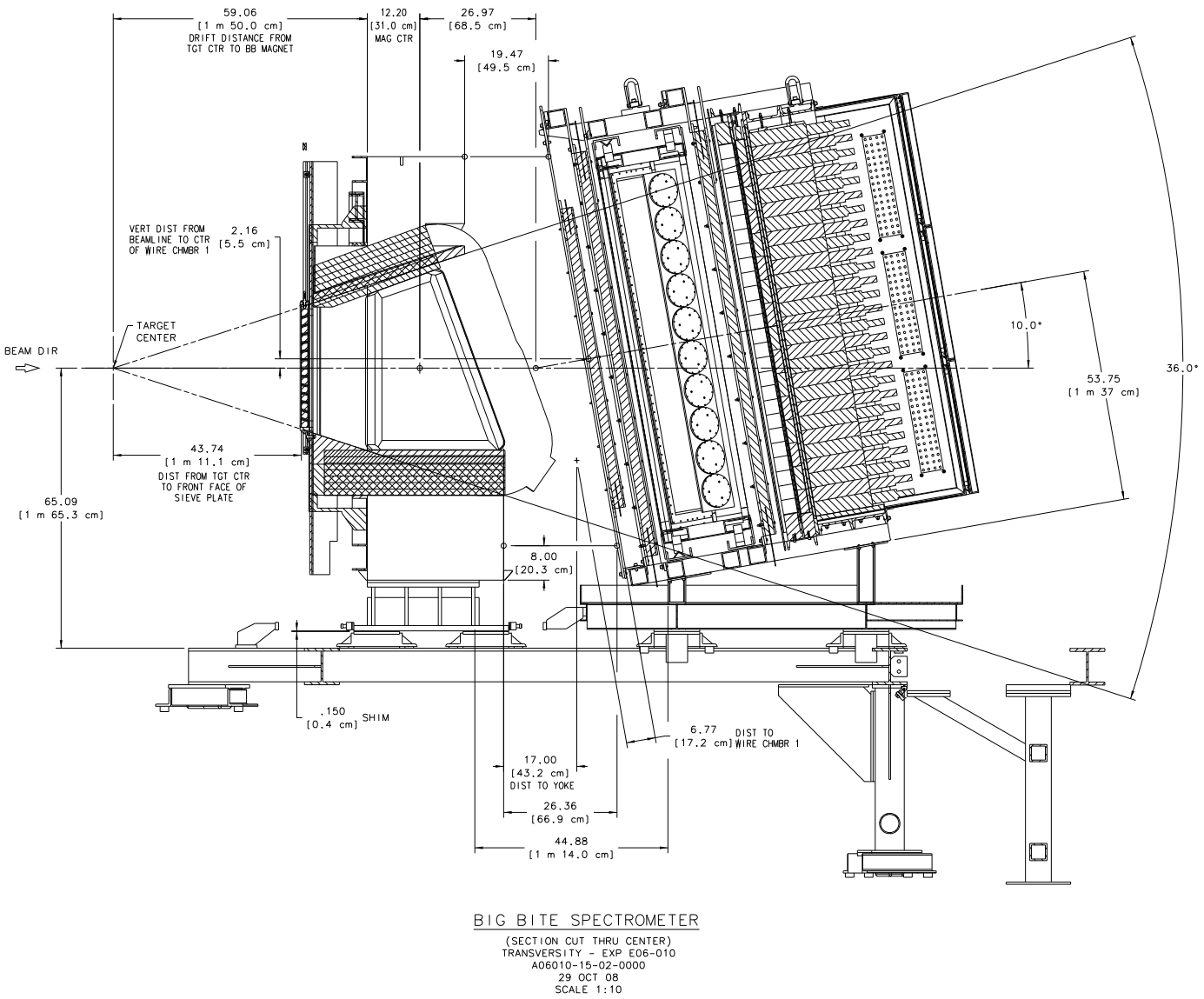

Figure 12: The BigBite dipole magnet and its electron detector package as in the Neutron Transversity experiment (E06-010).

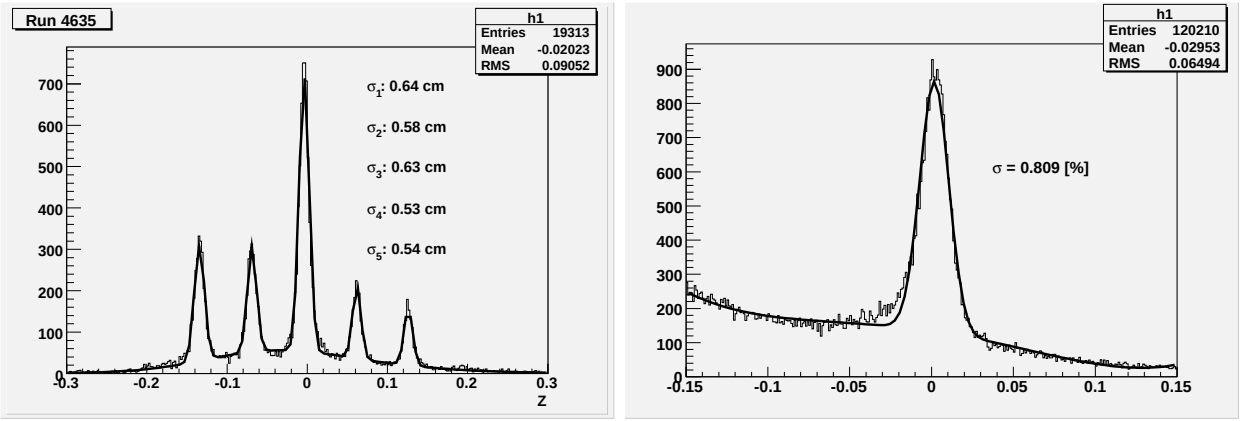

Figure 13: BigBite spectrometer online track reconstruction at 1.5m drift distance. Vertex resolution δz_{tar} on multi-carbon foil targets along the beam direction, on the left. Momentum resolution $\delta p/p$ in $p(e,e')$ elastic scattering calibration run, on the right.

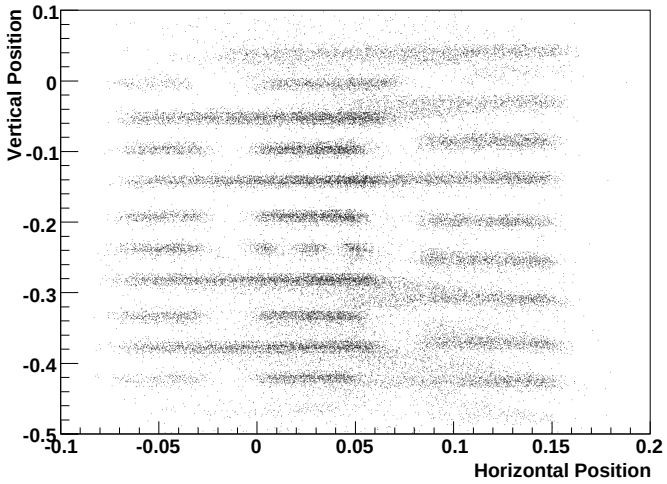

Figure 14: BigBite spectrometer online track reconstruction at 1.5m drift distance. Reconstructed track positions when a 1.5 inch thick "slot-slit" was inserted in front of the BigBite dipole magnet.

Single particle background rates on BigBite wire chamber

Based on a Monte Carlo simulation code GDINR [44], and the most recent operation experiences during Neutron Transversity, we estimated that the background rate on BigBite wire chambers to be around 20-30 MHz per plane, similar to the situation in Transversity, at an operation voltage of 1700 volts and a PreAmp card threshold of 4.4 volts. This typical chamber rate posses no special issues in chamber operation and track reconstruction.

A plan of BigBite detector improvements

Although the current BigBite detectors in the Netron transversity experiment is perfectly adequate for this proposal, we notes here that a plan of improvements is in

place for other Hall A experiments, especially for single-arm inclusive measurements. Relevant to this proposal we list the following planned improvements:

- Collimation and detector shielding.
  By pushing the BigBite magnet back to 1.7 m, extra space becomes available before the magnet to install lead collimators to better define the solid angle and stop low energy particles. In addition, unused space inside the magnet's opening, currently stuffed with wood at the top and the bottom, will be replaced by lead bricks. A detector shielding hut, made of one inch thick Aluminum plates, as well as an improved downstream beam pipe shielding will be installed. With the improved shielding, chamber rates are to be reduced to ~ 10 MHz per plane, make it possible to consider an increased luminosity.

- Detector re-arrangements and a spare chamber at the front.
  Due to the reduced BigBite solid angle in this experiment, the pre-shower+shower assembly can be moved back by 65 cm. A spare front chamber (the "UVa spare" or the "HamptonU spare") can be stacked with the current chamber-1 at the front while the current chamber-2 can be moved back to stack with chamber-3, make it a two-by-two tracking station each has 12 tracking planes.

- An improved gas Cherenkov detector.
  With the extra space available, the existing threshold gas Cherenkov detector can be modified to increase the gas passage to 80 cm from 40 cm. It is to be filled with CO_2 gas (n=1.00041, pion threshold 4.87 GeV/c). This modified gas Cherenkov is very similar to the existing HRS gas Cherenkov in geometrical size and expected performance. An average of 12 photo-electrons is expected, leading to an electron detection efficiency of $> 99\%$.

3.5 The hadron arm: left HRS+septum

The Hall A left HRS spectrometer with its septum magnet at 6° has been used in many experiments in the past, including the Hypernuclei, the Parity, the Small Angle GDH and the Pentaquark Search experiments. We chose to set HRS at 4.3 GeV/c, its maximum momentum, to strongly favor the current fragmentation by detecting the leading hadron at $z_h \approx 0.5$.

The optical properties of HRS+septum system, especially with an extended target, has been well-studied in the Small Angle GDH experiment (E97-110). As shown in Fig. 15, the interaction point resolution is $\delta z_{tar} \approx 2.0cm$. A Monte Carlo code was shown to reproduce the spectrometer's acceptance reasonably well for E97-110.

The HRS_L detector package in this experiment will include two scintillator planes for trigger, two VDC chambers for tracking, a threshold gas Cherenkov for particle identification, two aerogel Cherenkov detectors for kaon ID, and a shower counter consists of two layers of lead glass blocks to provide a π/e separation. We estimate

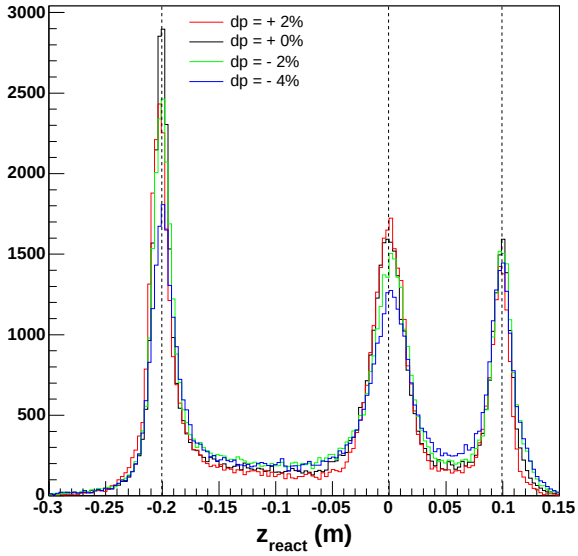

Figure 15: Interaction point resolution for HRS+Septum on carbon foil targets in experiment E97-110.

the single rate to be 10 kHz, and π^-/e^- ratio to be 5:1. By making a cut on the shower energy deposit alone, the electron contamination can be controlled to below 1% level in the π^- singles sample.

The standard gas Cherenkov detector, with a 0.8 m gas passage, will be filled with heavy gas C_4F_8O (n=1.00139) for this experiment. The corresponding momentum threshold is 2.64 GeV/c for pions, 9.34 GeV/c for kaons, and even higher for proton. For charged pion at 4.3 GeV/c momentum, the expected number of photo-electrons is well above 15 leading to a pion detection efficiency of $> 99\%$. Protons and kaons will be well-rejected. The cost of gas is \$4k per fill.

Two aerogel detectors A1 (n=1.015) and A2 (n=1.055), together with the threshold Cherenkov will provide $\pi/K/p$ separation, their momentum thresholds are shown in Fig. 16. At 4.3 GeV/c momentum, pions fire A1, A2 and gas Cherenkov. Kaons fire A1 and A2, but not the gas Cherenkov, protons fire A2, but not A1 nor gas Cherenkov.

Although it is not needed for the main physics goal of this experiment, efforts will be made to add extra kaon particle ID detector to improve kaon detection efficiency. The current RICH detector is designed to optimize π/K separation at 2.4 GeV/c. For this experiment at a momentum of 4.3 GeV/c, two modest-cost RICH solutions exist. The first solution is to refurbish the HERMES RICH detector which had been working well above 2.5 GeV/c. It is 126cm long and has an entrance window of 187cm×46cm which is slightly larger than the present Hall A RICH. The Hall A collaboration already has possession of this detector. The second solution is to upgrade the existing RICH detector by changing the liquid radiator to C_5F_{12} (cooling needed since it evaporate at 29°C), optimizing the drift gap to 50 cm, and increase

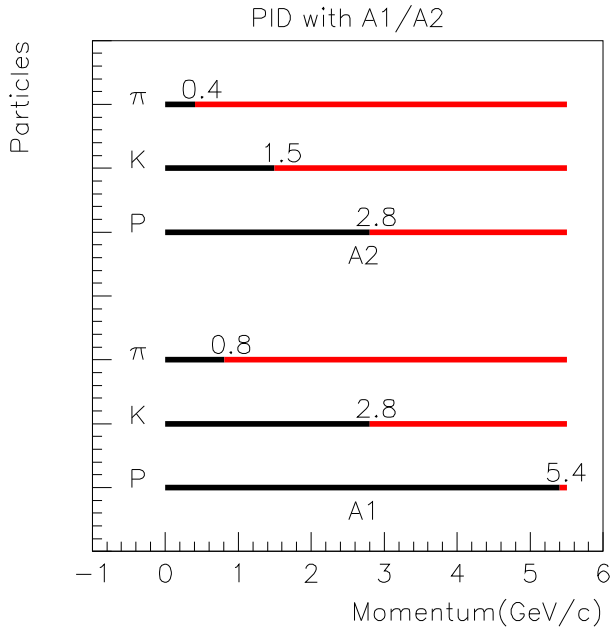

Figure 16: The Cherenkov thresholds for pions, kaons and protons in the two aerogel detectors.

the photon-detector size to 3.5 m^2 (three times larger than the present RICH). The estimated cost is about \$600k. It is expected that the current left-HRS focal-plane polarimetor chambers and the carbon-doors will be decommissioned, leaving plenty of space for new PID detectors. The Los Alamos group and the INFN group are interested in pursuing this option.

3.6 Trigger and offline event selection

The production trigger will be a coincidence between the left HRS (two scintillator plane AND) and the BigBite trigger (preshower and total energy AND). A coincidence time window of 100 ns will be wide enough to form the coincidence trigger. Offline flight-path corrected time-of-flight resolution is expected to be 1 ns. Coincidence $(e, e'p)$ events will have a 2 ns time delay compared with $(e, e'\pi)$ events, adding an extra layer of security in proton rejection. Since HRS+septum singles trigger rate is $\sim$ 10 kHz, and the BigBite singles trigger rate is $\sim$ 50 kHz, the raw accidental coincidence rate is less than 50 Hz. After the offline BigBite calorimeter ADC cut and the HRS_L PID cut, accidental coincidence events are not expected to survive at any significant level. Two-arm vertex consistency cut is expected to further eliminate the accidental events by an additional factor of 5, if there is any left. The true $(e, e'\pi)$ coincidence rate is $1 \sim 2$ Hz when all x-bins are summed over.

3.7 The polarized ^{3}He target

The Hall A polarized ^{3}He target has been successfully operated in many experiments over the last decade, including E94-010 and E95-001 in 1998, E99-117 and E97-103 in 2001, E97-110 and E01-012 in 2003, E02-013 in 2005 and the current running experiment E06-010 [42].

The polarized ^{3}He target used optically pumped Rubidium-Potassium vapor to polarize ^{3}He nuclei via spin-exchange. Three sets of Helmholtz coils provided a 25 Gauss holding field for any direction. Target cells were 40 cm long with a density of 10 amg (10 atm at 0°C). Beam currents on target ranged from 10 to 15 μA to keep the beam depolarization effect small and the cell survival time reasonably long (> 3 weeks). The luminosity is about 10^{36} nuclei/s/cm^2. The in-beam average target polarization achieved has been improved from $30 - 40\%$ in earlier experiments to 65% in the latest experiment. Two kinds of polarimetry, NMR and EPR (Electron-Paramagnetic-Resonance), were used to measure the polarization of the target. The uncertainty for each method is $\sim 2.5\%$ relative and the methods agreed well within errors.

Recent development effort has achieved a number of improvements. Most significant is the success of the K-Rb hybrid spin-exchange technique and using narrow-width lasers. Due to the much higher K-^{3}He spin exchange efficiency, the new hybrid cells have significantly shorter spin-up times and improved performance. Most of the cells have spin-up times of 5 hours (to be compared with > 10 hours for a typical Rb cell) and polarizations without beam $> 60\%$ (to be compared with $40 - 45\%$ for a typical Rb cell). The improved optical pumping efficiency coupled with reduced de-polarization effect by using narrow-width lasers have further improved the polarizations without beam to over 70%. The success rate of cell manufacturing has been also greatly improved.

A laser building next to the counting house was constructed prior to the G_E^n (E02-013) experiment to replace the laser hut in the hall. A new target lab with its infrastructure and safety interlock system was setup in the new laser building. With the laser building moved outside the hall, an optical fiber system was installed to transport laser light into the hall. Fifteen 75m-long optical fibers and three 5-to-1 combiners were installed. The typical light intensity drop through the optical fiber system is about 15%. Air cooling and a temperature interlock system are used to protect the fibers from over-heating. For one direction of optical pumping, about 90 watts of broad-width laser power or 60 watts of narrow-width laser power is needed. An automatic spin-flip system reverses the target spin direction once every 20 minutes.

A typical plot of on-line NMR target polarization measurements from E06-010 is shown in Fig. 17. Out of beam polarization reached 73% while in-beam polarization averaged to 65%. The polarized target system has gone through upgrades and improvements constantly. All the numbers we used for our rate estimate are based on achieved performance.

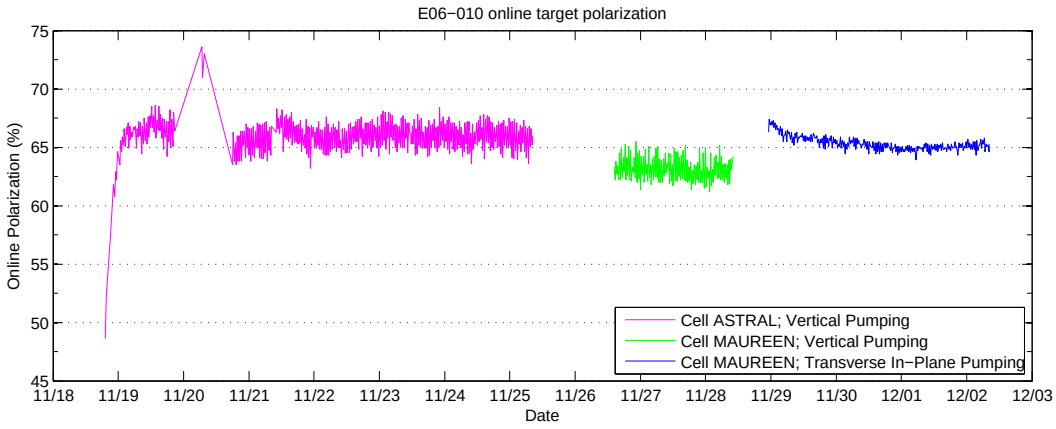

Figure 17: On-line NMR target polarization measurements during experiment E06-010.

In addition to the polarized ^{3}He target, the current target system has a multi-foil ^{12}C target for spectrometer optics study, a BeO target for beam tuning and a reference target cell. The reference cell consists of a 40-cm glass cell, which is identical to the polarized cell, connected to a gas handling system. The reference cell is used for calibration runs with Hydrogen, ^{3}He and Nitrogen gas, to measure dilution factor and to study systematic uncertainties.

4 Event Rate Estimate and Statistical Uncertainties

4.1 Cross section and rate estimate

The estimation of the coincidence cross sections has the following inputs:

- The inclusive $p(e,e')$ and $n(e,e')$ cross sections. Deep-inelastic cross sections for ^{3}He are assumed to be the sum of the two-protons plus one neutron, neglecting the nuclear effects in the intermediate x-region.
- Parametrizations of the fragmentation functions D_π^+, D_π^- and D_s^π for quark to pion fragmentation, D_K^+, D_K^- and D_d^K for quark to kaon fragmentation.
- A model of the transverse momentum distributions of pion and kaon as fragmentation products.

The inclusive deep inelastic (e,e') cross section can be expressed in the quark parton model as:

$$\frac{d^2\sigma}{d\Omega dE'} = \frac{\alpha^2(1+(1-y)^2)}{sxy^2}\frac{E'}{M_N\,\nu}\sum_{q,\bar{q}} e_q^2 f_1^q(x), \tag{32}$$

where $s = 2E\,M_N + M_N^2$. The unpolarized quark distribution functions $f_1^q(x)$ and $f_1^{\bar{q}}(x)$ are taken from the CTEQ5M global fits [45]. The semi-inclusive $(e,e'h)$ cross

section relates to the quark fragmentation function $D_q^h(z)$ and the total inclusive cross section σ_{tot} through:

$$\frac{1}{\sigma_{tot}}\frac{d\sigma(e,e'h)}{dz} = \frac{\sum_{q,\bar{q}} e_q^2 f_1^q(x) D_q^h(z)}{\sum_{q,\bar{q}} e_q^2 f_1^q(x)}. \tag{33}$$

For the quark to pion fragmentation functions $D_\pi^+(z)$ and $D_\pi^-(z)$, we follow the parametrization [46] of KKP to obtain the sum of $D_\pi^+(z) + D_\pi^-(z)$. For the ratio $D_\pi^-(z)/D_\pi^+(z)$, we use a fit [47] to the HERMES data [49]: $D_\pi^-/D_\pi^+ = (1-z)^{0.084}/(1+z)^{1.984}$. Fragmentation functions D_s^π, D_K^+, D_K^- and D_d^K in the KKP parametrization are used.

Existing data indicate that the fragmented products follow a Gaussian-like distribution in transverse momentum. For the $N(e,e'\pi)X$ reaction, HERMES data [48] showed that the transverse momentum ($P_\perp$) distribution for both π^+ and π^- follow the form of $e^{(-aP_\perp^2)}$ with $a = 3.76$ (GeV/c)$^{-2}$, corresponding to an average quark transverse momentum of $\langle P_\perp^2 \rangle = 0.26$ (GeV/c)^2. Charged kaon transverse momentum distributions are also found to be similar [48]. We used this distribution and realistic spectrometer acceptances in a Monte Carlo simulation to estimate the count rates. Hadron decay is considered in the rate estimation. The typical survival factors for $\pi^\pm$ and $K^\pm$ at 4.30 GeV/c are 0.90 and 0.45 respectively, after a flight-path of 26.0 m through the septum magnet and HRS.

4.2 Statistical uncertainties on raw asymmetries

Event rates, total number of events in each bin, statistical uncertainties of raw asymmetries are listed in Table–3 for the $(e,e'\pi)$ and the by-product $(e,e'K)$ reactions. We assumed a beam current of 15 μA, a beam polarization of 85%, a target length of 40 cm with a ^{3}He gas pressure of 10 atm, and a target polarization of 65%.

4.3 Statistical uncertainties on physics asymmetries and $\Delta d_v - \frac{1}{4}\Delta u_v$

The expected statistical uncertainties on ^{3}He physics asymmetries A_{1He}^h and $A_{1He}^{\pi^+\pm\pi^-}$ are listed in Table 4.

Physics asymmetries on ^{3}He are translated into neutron asymmetries A_{1n}^h and listed in Table 5 together with the corresponding dilution factors. An effective neutron polarization of 86.5% in ^{3}He ground state has been taken into account.

Statistical uncertainties on polarized parton distribution $\delta\left[x(\Delta d_v - \frac{1}{4}\Delta u_v)\right]_{CL}$ according to the leading order Christova-Leader (CL) method, uncertainty propagation following Eq. 11, are listed in Table 10.

$(e, e'\pi^{\pm})$ rates and total number of events on ^{3}He target:

$\langle x \rangle$	$\langle z_\pi \rangle$	R^{π^+} Hz	R^{π^-} Hz	N^{π^+} k	N^{π^-} k	$P_B P_T \mathcal{P}_{kin}$	$\delta A_\parallel^{\pi^+}$ %	$\delta A_\parallel^{\pi^-}$ %
0.110	0.43	0.82	0.59	1011.	467.	0.659	0.10	0.15
0.208	0.47	0.50	0.32	623.	256.	0.575	0.13	0.20
0.323	0.51	0.25	0.14	303.	113.	0.515	0.18	0.30
0.461	0.56	0.07	0.04	87.	30.	0.464	0.34	0.58

$(e, e'K^{\pm})$ rates and total number of events on ^{3}He target:

$\langle x \rangle$	$\langle z_K \rangle$	R^{K^+} Hz	R^{K^-} Hz	N^{K^+} k	N^{K^-} k	$P_B P_T \mathcal{P}_{kin}$	$\delta A_\parallel^{K^+}$ %	$\delta A_\parallel^{K^-}$ %
0.110	0.43	0.190	0.121	236.	95.	0.659	0.21	0.32
0.208	0.47	0.117	0.061	146.	48.	0.575	0.26	0.46
0.323	0.51	0.059	0.025	74.	20.	0.515	0.37	0.70
0.461	0.56	0.018	0.006	22.	5.	0.464	0.67	1.41

Table 3: Pion and kaon event rates (R^h), the total number of events (N^h), the product of kinematic factor, beam and target polarization ($P_B P_T \mathcal{P}_{kin}$), the expected statistical uncertainties of raw asymmetry ($\delta A_\parallel^h$) are listed. Data of all x-bins will be collected simultaneously.

4.4 Statistical uncertainties on moment of $\Delta d_v - \frac{1}{4}\Delta u_v$

From Table 10 for the measured x-region, we obtain the statistical uncertainty of first moment,

$$\delta \left[\int_{0.110}^{0.461} (\Delta d_v - \frac{1}{4}\Delta u_v) dx \right]_{LO} = \pm 0.023 \ (stat.) \tag{34}$$

4.5 Systematic uncertainties

Systematic uncertainty of A_{1He}^h and A_{1n}^h

Knowledge of target polarization and dilution factor dominates the systematic uncertainty of A_{1n}^h. The effects of radiative corrections will be treated in a Monte Carlo simulation following the procedures of the HERMES analysis [2], which found that the systematic uncertainties introduced by this procedure are negligible. Kinematic smearing will also be treated following the procedure of the HERMES analysis.

Major systematic uncertainties on A_{1He}^h:

Target polarization $\delta P_T / P_T$:	$\pm 2.5\%$ relative
Beam polarization $\delta P_B / P_B$:	$\pm 2.0\%$ relative
Helicity correlated beam charge uncertainty $\delta(Q_+/Q_-)$:	$\ll 10^{-4}$ absolute
Radiative correction and kinematic smearing:	$\pm 1.5\%$ relative
Knowledge of R and correction from $A_\perp$:	$\pm 1.5\%$ relative

$\langle x \rangle$	$\delta A_{1He}^{\pi^+}$ %	$\delta A_{1He}^{\pi^-}$ %	$\delta A_{1He}^{K^+}$ %	$\delta A_{1He}^{K^-}$ %	$\delta A_{1He}^{\pi^+ + \pi^-}$ %	$\delta A_{1He}^{\pi^+ - \pi^-}$ %
0.110	0.15	0.22	0.31	0.49	0.13	0.81
0.208	0.22	0.34	0.46	0.79	0.19	0.88
0.323	0.35	0.58	0.72	1.37	0.31	1.18
0.461	0.73	1.25	1.44	3.03	0.64	2.13

Table 4: The statistical uncertainties of double-spin asymmetry $A_{1He}^h(\vec{n}+2p)$ for ^{3}He in which the effective neutron polarization in the ^{3}He ground state (86.5%) has been taken into account.

$\langle x \rangle$	f^{π^+}	f^{π^-}	$\delta A_{1n}^{\pi^+}$ %	$\delta A_{1n}^{\pi^-}$ %	f^{K^+}	f^{K^-}	$\delta A_{1n}^{K^+}$ %	$\delta A_{1n}^{K^-}$ %
0.110	0.277	0.331	0.63	0.78	0.287	0.332	1.26	1.71
0.208	0.238	0.313	1.07	1.27	0.250	0.312	2.11	2.94
0.323	0.197	0.292	2.07	2.28	0.210	0.278	3.95	5.68
0.461	0.162	0.283	5.19	5.08	0.171	0.251	9.74	13.98

Table 5: The expected statistical uncertainties of the double-spin asymmetry A_{1n}^h and the corresponding dilution factors.

Total systematic uncertainty on A_{1He}^h $\pm 3.8\%$ **relative**

Extra systematic uncertainties involved in extracting A_{1n}^h:
Dilution factor $\delta f/f$: $\pm 2.5\%$ relative
Effective neutron polarization in ^{3}He $\delta P_n/P_n$: $\pm 4.2\%$ relative
Systematic uncertainty on A_{1n}^h (exp.+theory): $\pm 6.2\%$ **relative**

Taken the values of A_{1He}^h from the NLO best fit (KRE set), the systematics uncertainties are listed in Table-7. The systematics uncertainties of A_{1n}^h are listed in Table-8.

When extracting $x(\Delta d_v - \frac{1}{4}\Delta u_v)$ the knowledge of unpolarized PDF ($\delta q/q \approx \pm 4\%$) contributes to the systematic uncertainties. Theoretical uncertainties (PDF and ^{3}He to neutron correction) dominate the systematics in Δd_v, as listed in Table-9.

$\langle x \rangle$	$\langle Q^2 \rangle$ GeV^2	xu_v	xd_v	$\delta\left[x(\Delta d_v - \frac{1}{4}\Delta u_v)\right]_{CL}$	$\delta(\Delta d_v - \frac{1}{4}\Delta u_v)_{CL}$
0.110	2.06	0.570	0.301	0.009	0.085
0.208	3.61	0.671	0.303	0.012	0.056
0.323	5.15	0.557	0.209	0.013	0.039
0.461	6.70	0.325	0.095	0.013	0.029

Table 6: The expected statistical uncertainties of $\delta\left[x(\Delta d_v - \frac{1}{4}\Delta u_v)\right]_{CL}$ according to the leading order Christova-Leader (CL) method. Values of $xu_v(x)$ and $xd_v(x)$ from CTEQ are also listed.

	Stat. Uncert.			Sys. Uncert.		
$\langle x \rangle$	$\delta A_{1He}^{\pi^+}$ %	$\delta A_{1He}^{\pi^-}$ %	$\delta A_{1He}^{\pi^+-\pi^-}$ %	$\delta A_{1He}^{\pi^+}$ %	$\delta A_{1He}^{\pi^-}$ %	$\delta A_{1He}^{\pi^+-\pi^-}$ %
0.110	0.15	0.22	0.81	0.12	0.05	0.42
0.208	0.22	0.34	0.88	0.13	0.03	0.35
0.323	0.35	0.58	1.18	0.11	0.01	0.32
0.461	0.73	1.25	2.13	0.09	0.05	0.22

Table 7: Systematic uncertainties of A_{1He}^h are compared with statistical uncertainties.

	Stat. Uncert.		Sys. Uncert.	
$\langle x \rangle$	$\delta A_{1n}^{\pi^+}$ %	$\delta A_{1n}^{\pi^-}$ %	$\delta A_{1n}^{\pi^+}$ %	$\delta A_{1n}^{\pi^-}$ %
0.110	0.63	0.78	1.10	1.00
0.208	1.07	1.27	1.38	1.25
0.323	2.07	2.28	1.39	1.25
0.461	5.19	5.08	1.12	1.02

Table 8: Systematic uncertainties of A_{1n}^h are compared with statistical uncertainties.

Therefore, over the measured region, we have:

	Stat. Uncert.	Systematic Uncert.		
$\langle x \rangle$	$\delta \left[x(\Delta d_v - \frac{1}{4}\Delta u_v)\right]_{CL}$	exp.	theory	total
0.110	0.009	0.007	0.010	0.012
0.208	0.012	0.008	0.011	0.014
0.323	0.013	0.007	0.011	0.013
0.461	0.013	0.005	0.009	0.010

Table 9: Systematic uncertainties of $\delta\left[x(\Delta d_v - \frac{1}{4}\Delta u_v)\right]_{CL}$ for the leading order Christova-Leader method.

$$\delta\left[\int_{0.110}^{0.461}(\Delta d_v - \frac{1}{4}\Delta u_v)dx\right]_{LO} = \pm 0.023\ (stat.) \pm 0.025\ (sys.) \tag{35}$$

Recall that from Eq. 25, if the moment of $\Delta d_v - \Delta u_v$ can be pinned down to ± 0.05, the moment of polarized sea asymmetry can be constraint to $\delta\left[\int(\Delta\bar{u} - \Delta\bar{d})dx\right] = \pm 0.025$, eight standard deviations from the prediction of Chiral Quark soliton model.

This result on the valence quark moment is to be compared with the COMPASS deuteron results [5] at $Q^2 = 10.0$ GeV^2:

$$\left[\int_{0.006}^{0.7}(\Delta u_v + \Delta d_v)dx\right]_{LO} = 0.40 \pm 0.07\ (stat.) \pm 0.06\ (sys.) \tag{36}$$

Systematic uncertainty $\Delta\bar{u} - \Delta\bar{d}$

To further extract $\Delta\bar{u} - \Delta\bar{d}$ according to Eq. 20, knowledge of $\Delta u_v - \Delta d_v$ is needed. Of course, the best option is to perform measurements on three different polarized targets (proton, deuteron and ^{3}He) within the same experimental set up, such that consistency checks are possible to set limits on systematic uncertainties of $\Delta u_v - \Delta d_v$.

Given the large installation overhead of handling two types of polarized targets, we propose here to follow the "second best" option. The neutron (^{3}He) data from this experiment, or $\Delta d_v - \frac{1}{4}\Delta u_v$, can be combined with the world data on polarized proton target, to obtain the best knowledge of $\Delta u_v - \Delta d_v$.

Assuming the world data of Δu_v will reach the similar statistical and systematic uncertainties of this experiment, Table 10 lists the uncertainties on $x(\Delta\bar{u} - \Delta\bar{d})_{LO}$. Uncertainties due to the eisting knowledge [20,15] of inclusive $g_1^p(x, Q^2)$ and $g_1^n(x, Q^2)$ ($\delta g_1^p = 0.0059$, $\delta g_1^n = 0.0057$) are also included. We note that improvements from the inclusive data set of CLAS12 and this experiment will further constrain $g_1^p(x, Q^2)$ and $g_1^n(x, Q^2)$.

$\langle x \rangle$	$\frac{1}{2}\delta x(\Delta u_v - \Delta d_v)$	$3x\delta g_1^p$	$3x\delta g_1^n$	$\delta\left[x(\Delta\bar{u} - \Delta\bar{d})\right]$	
	stat.	stat.	stat.	stat.	sys.
0.110	0.007	0.002	0.002	0.007	0.009
0.208	0.008	0.004	0.004	0.010	0.010
0.323	0.009	0.006	0.006	0.012	0.009
0.461	0.009	0.008	0.008	0.015	0.007

Table 10: Statistical and systematic uncertainties of $x(\Delta\bar{u} - \Delta\bar{d})_{LO}$.

Effective nucleon polarization in ^{3}He

Effective nucleon polarization in ^{3}He for deep-inelastic scattering gives:

$$g_1^{^3He} = P_n g_1^n + 2P_p g_1^p \tag{37}$$

where $P_n(P_p)$ is the effective polarization of the neutron (proton) inside ^{3}He [51]. These effective nucleon polarizations $P_{n,p}$ can be calculated using ^{3}He wave functions constructed from N-N interactions, and their uncertainties were estimated using various nuclear models [50,51,52,53], giving

$$P_n = 0.86^{+0.036}_{-0.02} \quad and \; P_p = -0.028^{+0.009}_{-0.004} \; . \tag{38}$$

The small proton effective polarization (2.8%) causes small offsets in the ^{3}He asymmetries, compared to that from a free neutron. The uncertainties associated with this small offset are even smaller when considering that the corresponding proton asymmetries are better known and will be improved in the coming years.

At $x = 0.110 \sim 0.461$, especially around $x = 0.3$, the nuclear EMC effect becomes rather small, as has been demonstrated on many different nucleus.

π-N final state interaction

Since pions carry no spin, πN final state interactions will not introduce asymmetries in A^h_{1He}. Effect of π-N final state interaction will come through the dilution factors. By measuring the leading pions at 4.3 GeV/c, where the π-N total cross sections are reasonably flat, effects of FSI are minimized. A detailed π-N re-scattering calculation [54] confirmed that the modifications to the cross section are rather small at this kinematics.

Target fragmentation and vector meson production

In principle, intermediate ρ production processes are part of the fragmentation process and should not be subtracted from the SIDIS cross sections. Furthermore, due to the charge conjugation, the effect of intermediate ρ^0 production is canceled in observables related to $\pi^+ - \pi^-$. Therefore, the Christova-Leader method of flavor decomposition is not sensitive to ρ production.

At a high-z setting of this experiment ($z \approx 0.5$), target fragmentation contamination is expected to be small, as has been shown by the HERMES LUND based Monte Carlo simulation. In addition, in the $\pi^+ - \pi^-$ yield target fragmentation contributions are mostly canceled.

Corrections from non-vanishing $A^n_\perp$ (or A^n_{LT})

Since the target polarization is along the beam direction, not exactly along the virtual photon direction $\theta_{\gamma^\star}$, measurements of $A_\parallel$ should in principle be corrected by a small contribution from $A_\perp$ in order to obtain the physics asymmetry A^h_{1N}. In this experiment, we have $\sin\theta_{\gamma^\star} \approx 0.1$, therefore, the uncertainty associated with this correction is of the order $0.1 \times (\delta A^n_\perp)$.

In the published HERMES and SMC data, the corrections from $A_\perp$ were neglected based on the observation that in inclusive DIS $g_2(x)$ turned out to be rather small. The residual effect of non-vanishing g_2 (or $A_\perp$) in SIDIS has been included in the estimation of systematic uncertainties in the HERMES case. The contribution to the fractional systematic uncertainties on A^h_{1N} was estimated to be 0.6% for proton and 1.4% for deuteron.

- The leading order contribution in $A_\perp$ (or A_{LT} in Mulders' notation) is modulated by an angular dependence of $\cos(\phi_s - \phi_h)$. When a reasonable range of ϕ_h is covered, as in this experiment, the averaged contribution from $A_\perp$ will most likely to be washed out.

- Aside from the angular modulation, $A_\perp$ was predicted to be at the 10% level for the proton in bag-model calculations (Mulders, Yuan). Assuming $A^n_\perp$ is at the similar level, the correction to A^h_{1n} will be at 1% level for this experiment, much less than the statistical uncertainties.

- The value of $A_\perp$ will likely to be determined to much better than 10% in the next few years. The Hall A Neutron Transversity experiment [42] (E06-010), with a transversely polarized ^{3}He target, will provide information on $A_\perp^n$ within the next year.

Based on the above consideration, we feel confident that even without dedicated transverse target runs the systematic uncertainties associated with $A_\perp^n$ correction will be much less compared to the statistical uncertainties of this experiment.

5 Beam time request, hardware costs and installation time

5.1 Beam time request

The beam time request are listed in Table 11. The relative time between π^+ and π^- runs are chosen to minimize the uncertainty of $A_{1He}^{\pi^+-\pi^-}$ for the $x = 0.208$ bin. We request 672 hours (28 days) of total beam time, of which 564 hours is for beam on the polarized ^{3}He target, 48 hours is for detector shakedown. Considerable overhead time (60 hours total) is requested. This overhead time can be shared between activities such as Möller measurements, unpolarized target runs, and target polarization measurements. Major target related down times can also be arranged to coincide with scheduled accelerator maintenance.

	Time-h^+ hour	Time-h^- hour
Production	**344**	**220**
Beam on polarized target	**564**	
Optics check and detector shakedown	**48**	
Overhead, Möller runs and reference cell runs.	**60**	
Total Time Request	**672 (28 days)**	

Table 11: Details of the beam time request.

5.2 Hardware costs and installation time needed

The existing septum magnet's support table, originally designed to accommodate two septa magnets, need to be re-made for a single septum support to avoid interference with the BigBite spectrometer. The cost of the new table is \$12k. The front legs of the BigBite support frame, originally designed to be moved around the pivot, need to be modified to accommodate the interaction point's 80 cm upstream shift introduced by the use of septum magnet. The cost of this modification is \$18k.

The overall installation time needed for this experiment is four to six weeks. Installation of the standard polarized ^{3}He target in conjunction with the left septum magnet can be accomplished within four weeks. Installation time for the BigBite spectrometer is four to six weeks.

6 The Expected Results

6.1 Double spin asymmetries A^h_{1He} and A^h_{1n}

The expected statistical accuracies of semi-inclusive double-spin asymmetries are shown in Fig. 19 as functions of x. HERMES and SMC deuteron asymmetries are translated into neutron asymmetries, according to the leading order cross section assumption, and plotted as a comparison.

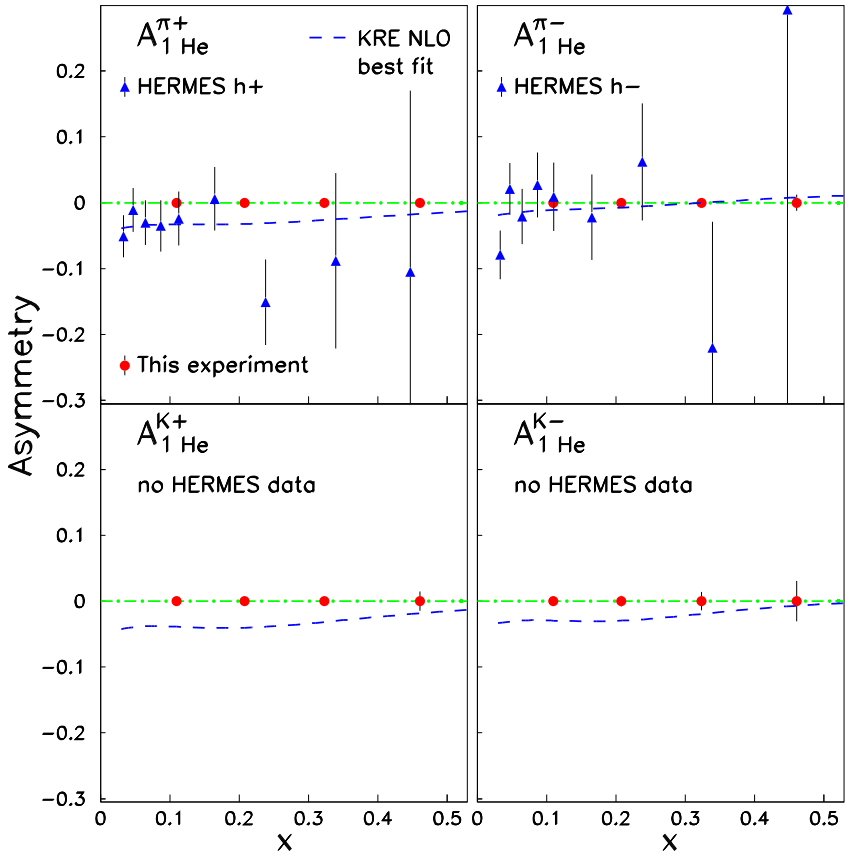

Figure 18: The expected statistical accuracy of pion and kaon semi-inclusive physics asymmetries on ^{3}He. The HERMES 1997 data on a polarized ^{3}He target obtained without hadron PID [2] are also shown as a comparison. The next-to-leading order "best fit" results corresponding to the Kretzer fragmentation function [55] (KRE) are show as dashed curves.

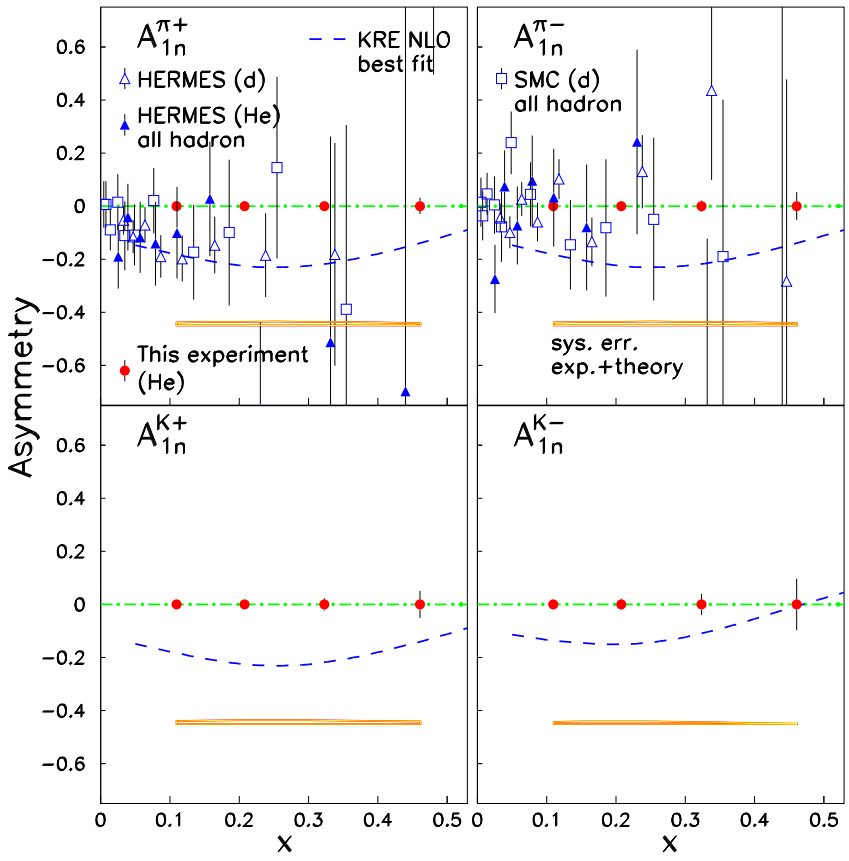

Figure 19: The expected statistical accuracy of asymmetries corresponding to "a free neutron target" $A_{1n}^{\pi^+}$, $A_{1n}^{\pi^-}$, $A_{1n}^{K^+}$ and $A_{1n}^{K^-}$ as functions of x. HERMES results[2] on the deuteron target are also shown. The next-to-leading order "best fit" results corresponding to the Kretzer fragmentation[55] (KRE) are show as dashed curve.

6.2 Flavor decomposition of quark polarization and the impacts to NLO global fits

$\Delta d_v(x)$ from the leading-order Christova-Leader method

Statistical accuracies of $x\Delta d_v$ from this experiment, according to the leading order Christova-Leader method, are plotted in Fig. 20. The published data from HERMES, which used the purity method and included inclusive asymmetry data, are also plotted. When the HERMES data were analyzed following the Christova-Leader method, dramatic increase in statistical uncertainties can not be avoid due to the unfavorable cross section ratio of $\sigma^{\pi^-}/\sigma^{\pi^+}$ in the HERMES kinematics (see Fig. 27 in Appendix). The SMC data, which assumed symmetric sea polarization, are also shown.

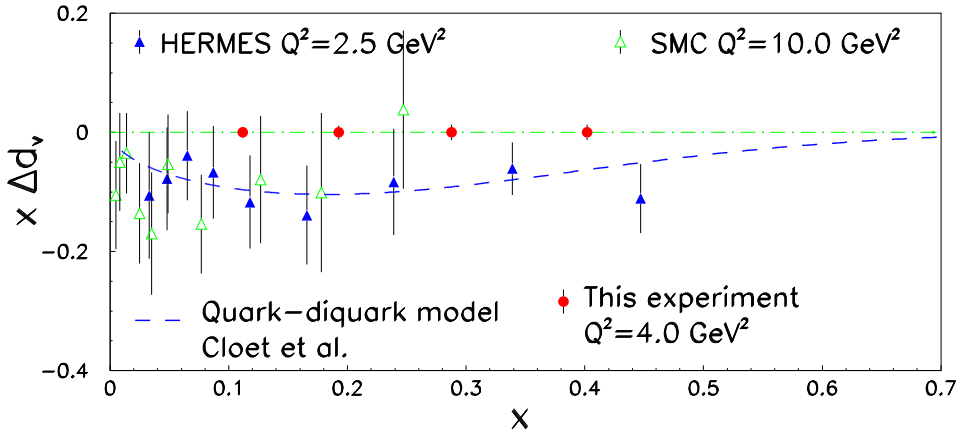

Figure 20: The expected statistical accuracy of $x\Delta d_v$. The published HERMES purity results [2,3], which included a combined data set of inclusive and semi-inclusive asymmetries, are also shown.

$\Delta\bar{u}(x) - \Delta\bar{d}(x)$ from the leading-order Christova-Leader method

When combined with the expected world proton data to obtain $\Delta u_v - \Delta d_v$, this experiment will be sensitive to the polarized sea asymmetry $\Delta\bar{u}(x) - \Delta\bar{d}(x)$, as shown in Fig. 21 together with several theory predictions.

Impact to NLO QCD global fit: sea and gluon polarization moments

When the impacts to NLO QCD fit were studied, we have assumed a target polarization of 42% instead of 65%. An update of impacts study is in progress as of December-2008. The following results were obtained with 50% larger projected error bars on A_{1n}^h.

Constraints to the moments of $\Delta\bar{u}$, $\Delta\bar{d}$ and Δs with the expected ^{3}He data in the next-to-leading order global fit [11] are shown in Fig. 22. The constraint on Δg moments coming from the addition of data of this experiment, as shown in Fig. 23,

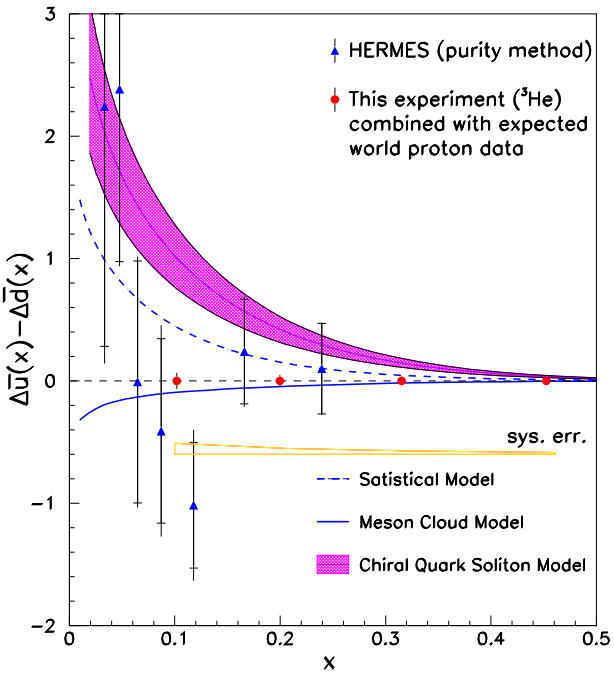

Figure 21: When combined with the expected world proton data, the expected statistical accuracy of $\Delta\bar{u} - \Delta\bar{d}$ is plotted. The published HERMES purity results [2], which included a combined data set of inclusive and semi-inclusive asymmetries, are also shown. Model predictions are from the Statistical Model [40], Meson Cloud Model [18] and the Chiral Quark Soliton Model [37].

is as stringent as the $A_{LL}^{\pi^0}$ data from PHENIX at RHIC-2006 run [13]. The main reason of this sensitivity is because Δg is obtained in the global fit through the Q^2-evolutions, but always coupled with the sea distribution. Once the sea distribution can be reasonably fixed with the semi-inclusive data, gluon polarization is better constrained through the global fit. The impact to the moment of u and d-quark polarization is shown in Fig. 24.

7 Relation with other experiments

- A polarized proton target (NH_3) measurement in Hall A at the same kinematics will be very attractive in terms of reducing systematic uncertainties in $\Delta u_v - \Delta d_v$, thus $\Delta\bar{u} - \Delta\bar{d}$. For such a measurement using the same set up as in this proposal, a beam time of ~50 days is needed to reach a comparable accuracies on $A_{1p}^{\pi^+-\pi^-}$ and therefore $\Delta u_v - \frac{1}{4}\Delta d_v$. A planned 6 GeV experiment in Hall A (g2p experiment, E08-027, A. Camsonne, J.P. Chen and K. Slifer co-spokespersons) calls for the installation of the UVa polarized target. A success of such an experiment will certainly pave the way for future SIDIS measurements using the UVa polarized target in Hall A. Pending on the solutions of several technical issues regarding, a follow up proposal on proton target is likely to be submitted to a future PAC.

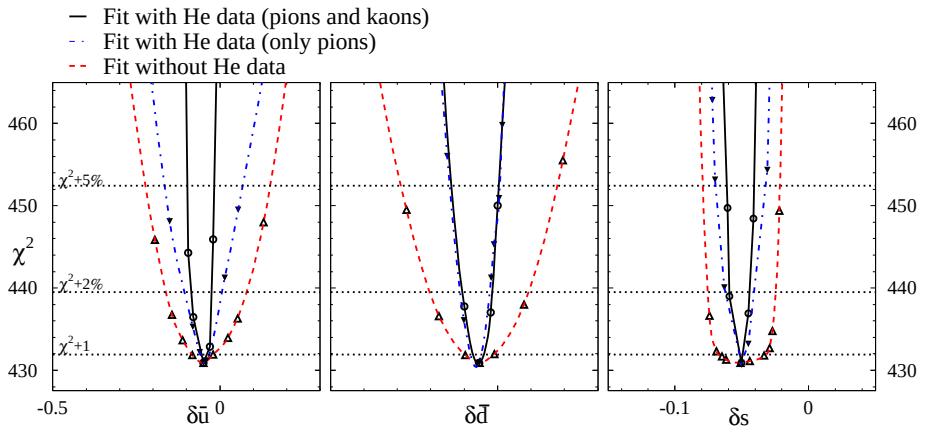

Figure 22: The constraints to the moments of sea polarization in NLO global fit by this experiment [11]. The red dashed lines are the constraint by the existing data, the blue dot-dashed lines are the constraints by adding the pion data from this experiment, the solid lines are the constraints by adding both pion and kaon data of this experiment. The horizontal dotted lines are corresponding to an overall χ^2 change of $\chi^2 + 1$ ($\pm 1\sigma$ in pPDF), $\chi^2 + 2\%$ and $\chi^2 + 5\%$ in the global fit.

- CLAS12 has planned SIDIS measurements on polarized proton and deuteron target using the large acceptance detector. It will be highly complimentary to this experiment. However, due to the 5 Tesla solenoid magnetic field at the interaction point of CLAS12, there's no practicle solution to install a polarized ^{3}He target so far. In addition, this experiment focus on a kinematics region of high-z_h, high-Q^2, high-W and high missing mass W' to strongly favor the current fragmentation region. The small angle access of the hadron spectrometer to align with $\vec{q}$ direction set this experiment apart from other possible arrangement at JLab. The capability to independently flip hadron arm's magnetic polarity is another unique advantage hard to match.

- HERMES published spin flavor separation results are considered as "final". There's no additional data available to improve statistics.

- The COMPASS experiment focus on high Q^2 at low-x, and on deuteron and proton targets, complimentary to this experiment.

- RHIC spin program. With the planned luminosity upgrade [14], RHIC will measure Δq through weak $W^{\pm}$ decays at $Q^2 = m_W^2$. Through evolution, valence quark densities at high-x and low-Q^2 region feeds into low-x and high-Q^2 region, providing a link to cross check results between this experiment and the RHIC results.

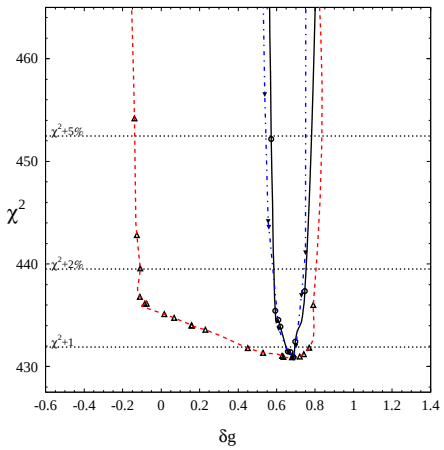

Figure 23: The constraint to the moment of the gluon polarizations in NLO global fit by this experiment, blue dot-dashed line: adding only pion data of this experiment, solid line: adding both pion and kaon data of this experiment.

8 Collaboration

Members of this collaboration have run many Hall A polarized ^{3}He target experiments and have been heavily involved in other Hall A BigBite experiments. We expect JLab will handle installation of the septum magnet and the BigBite spectrometer if it is not already in place from an earlier operation.

9 Summary

We propose to measure the beam-target double-spin asymmetries in semi-inclusive deep-inelastic $\vec{n}(\vec{e},e'\pi^+)X$ and $\vec{n}(\vec{e},e'\pi^-)X$ reactions (kaons as by-products) on a longitudinally polarized ^{3}He target, in the kinematic region of $x = 0.110 \sim 0.461$ at $Q^2 = 2.0 \sim 6.7$ GeV^2 with the leading hadron at $z \approx 0.5$. Since the neutron asymmetries are most sensitive to d-quark polarization, this experiment will dramatically improve our knowledge of Δd. The experiment will focus on the measurement of the combined asymmetry, $A_{1He}^{\pi^+-\pi^-}$. Based on the measurement of $A_{1He}^{\pi^+-\pi^-}$, valence density $\Delta d_v - \frac{1}{4}\Delta u_v$ will be extracted independently at leading order . When combined with the expected world data on proton (Δu_v) this experiment will provide the opportunity to address polarized sea asymmetry. The high precision data from this experiment will also be used as inputs to a global next-to-leading order QCD analysis to constrain quark helicity distributions, and indirectly the gluon polarization.

The BigBite spectrometer, in the same detector configuration as in the Neutron Transversity experiments, will be used to detect the scattered electrons at 25°. The left-HRS spectrometer, with its septum magnet at 6°, will be used to detect the leading hadrons in coincidence (at $p_h = 4.3$ GeV/c, $z \approx 0.5$). Since all experimental apparatus exist and operational, this experiment can be the first commissioning experiment in Hall A with 11 GeV beam. A total of 28 days of beam time at 11

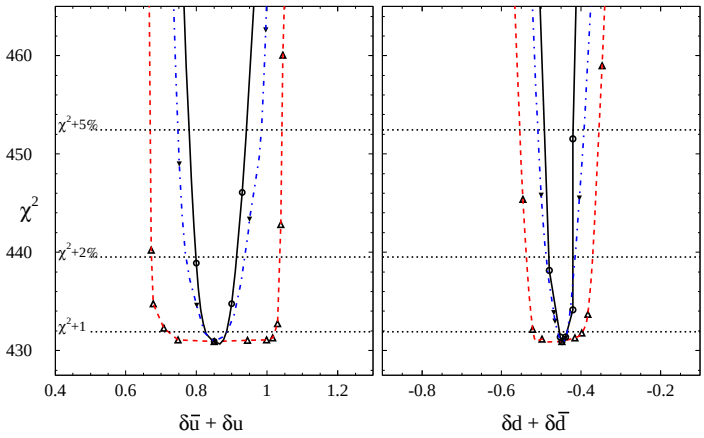

Figure 24: The constraints to the moments of u and d-quark polarization in NLO global fit by this experiment [11]. The red dashed lines are the constraint by the existing data, the blue dot-dashed lines are the constraints by adding the pion data from this experiment, the solid lines are the constraints by adding both pion and kaon data of this experiment.

GeV is requested in Hall A.

A Summary of HERMES purity method and results, and COMPASS results

The HERMES analysis explicitly assumed the $x - z$ factorization of Eq. 1 at the leading order, the asymmetries are related to the parton polarizations through linear relations as:

$$A_{1N}^h(x, Q^2, z) = \frac{\sum_f e_f^2 \Delta q_f(x, Q^2) \cdot D_f^h(z, Q^2)}{\sum_f e_f^2 q_f(x, Q^2) \cdot D_f^h(z, Q^2)}. \tag{39}$$

The HERMES analysis used the "purity method" to achieve leading order flavor decomposition [56]. In Eq. 39, a "purity matrix" $\mathcal{P}_f^h(x, Q^2, z)$ was defined such that:

$$A_{1N}^h(x, Q^2, z) \equiv \sum_f \mathcal{P}_f^h(x, Q^2, z) \cdot \frac{\Delta q_f(x, Q^2)}{q_f(x, Q^2)}, \tag{40}$$

where

$$\mathcal{P}_f^h(x) = \frac{e_f^2 q_f(x) \int dz D_f^h(z)}{\sum_i e_i^2 q_i(x) \int dz D_i^h(z)}, \tag{41}$$

and the explicit Q^2 notation has been omitted for simplicity. The "purity method" integrates over all the experimentally allowed z-range such that SIDIS events are included as much as possible to improve statistical accuracy. The exact values of $\mathcal{P}_f^h(x, Q^2, z)$ in the HERMES analysis were obtained through a detailed Monte Carlo simulation which was based on the Lund fragmentation model [57] and take into account the experimental phase space and detector efficiencies. The parameters used in the fragmentation model were fine-tuned in order to reproduce the measured hadron yields.

Integrating over hadrons with $0.2 < z < 0.8$, HERMES extracted five flavor quark polarizations:

$$\vec{Q} = \left(x\Delta u, x\Delta d, x\Delta \bar{u}, x\Delta \bar{d}, x\Delta s\right), \tag{42}$$

from a data base of measured double-spin asymmetries

$$\vec{A} = \left(A_{1p}^{\pi^+}, A_{1p}^{\pi^-}, A_{1d}^{\pi^+}, A_{1d}^{\pi^-}, A_{1d}^{K^+}, A_{1d}^{K^-}, A_{1p}, A_{1d}\right) \tag{43}$$

by solving the relations of $\vec{A} = \mathcal{P}_f^h(x) \cdot \vec{Q}$. The HERMES data on proton and deuteron asymmetries [2] are shown in Fig. 25 and 26 in comparison with the SMC data [4].

An independent effort of flavor decomposition using the leading order Christova-Leader method has also been carried out in the HERMES analysis [3], although not presented in the published data. However, due to the unfavorable π^-/π^+ ratio at higher-x bins in HERMES, the statistical uncertainties of the Christova-Leader method are rather large compared to that of the purity method, as shown in Fig. 27

Recently, the COMPASS experiment [5] released the results of $A_d^{h^+}$ and $A_d^{h^-}$, identified charged hardon asymmetries off a deuteron target, with improved statistical precisions at lower-x region. The asymmetry results are shown in Fig. 28.

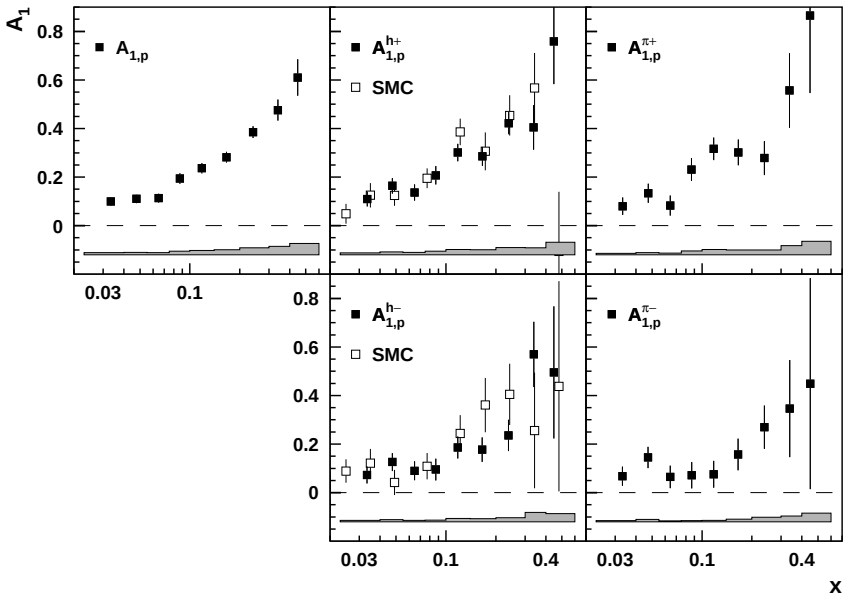

Figure 25: The double-spin asymmetries on proton A_{1p}^h form HERMES [2] and SMC [4].

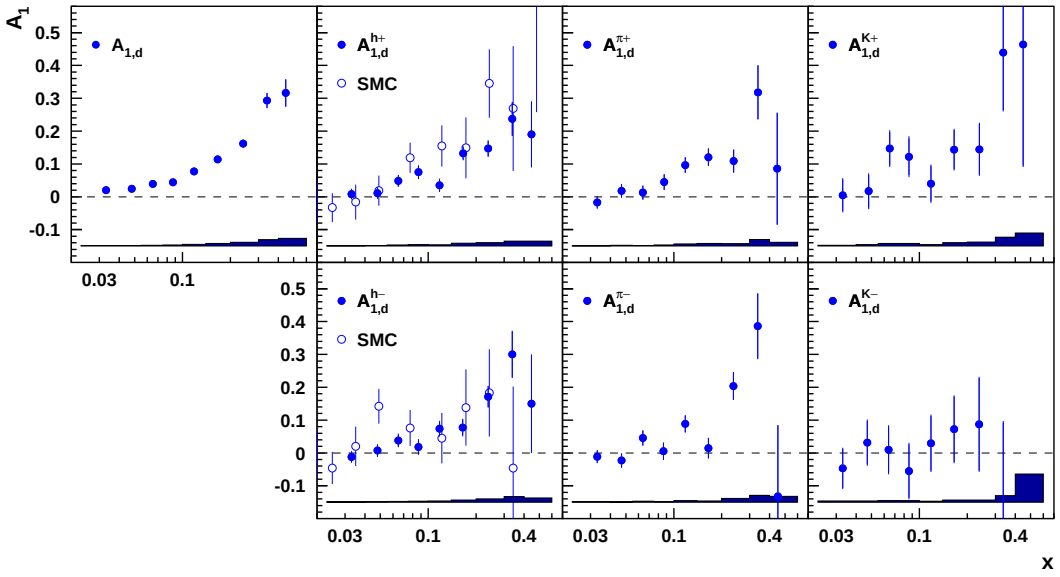

Figure 26: The double-spin asymmetries on deuteron A_{1d}^h form HERMES [2] and SMC [4].

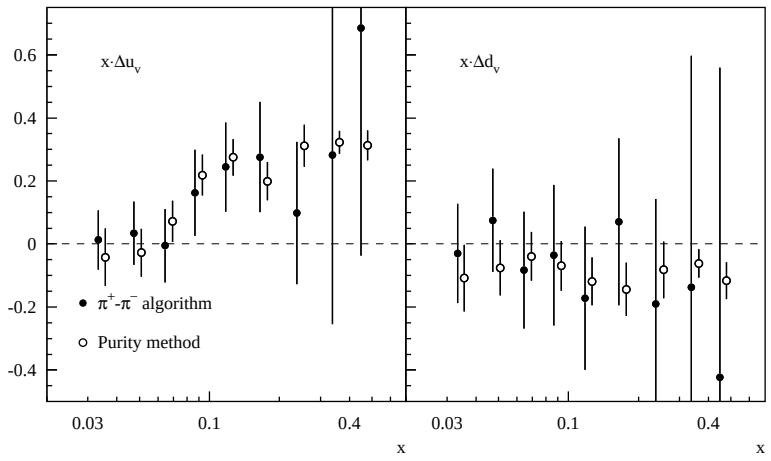

Figure 27: Statistical error comparison of the HERMES purity method (open circles) with the HERMES Christova-Leader method analysis [3] (solid circles).

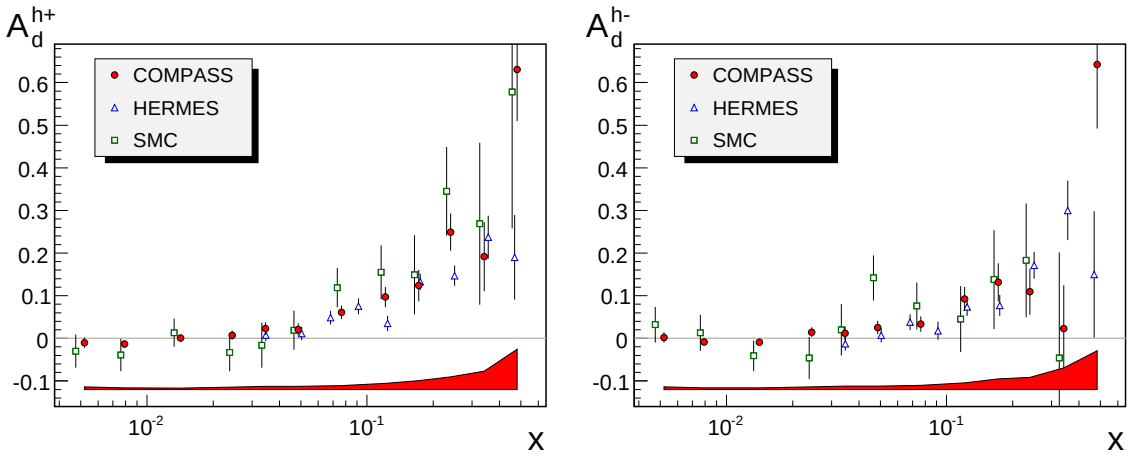

Figure 28: Hadron asymmetry $A_d^{h^+}$ and $A_d^{h^-}$ measured by COMPASS [5], SMC and HERMES.

B Leading-order SIDIS asymmetries

Following the short-hand notation of Ref[9], we take the spin-independent cross section as:

$$\sigma^h(x,z) = \sum_f e_f^2 q_f(x) \cdot D_{q_f}^h(z), \tag{44}$$

and the spin-dependent cross section as:

$$\Delta\sigma^h(x,z) = \sigma_{++}^h - \sigma_{+-}^h = \sum_f e_f^2 \Delta q_f(x) \cdot D_{q_f}^h(z), \tag{45}$$

where σ_{ij}^h refers to an electron of helicity-i and nucleon of helicity-j. Assuming isospin symmetry and charge conjugation invariance, the number of quark to pion fragmentation functions is reduced to three types: the favored (D_π^+), the unfavored (D_π^-) and the s-quark (D_s^π) fragmentation functions:

$$\begin{aligned} D_\pi^+ &\equiv D_u^{\pi^+} = D_{\bar{d}}^{\pi^-} = D_{\bar{u}}^{\pi^-} = D_{\bar{d}}^{\pi^+}, \\ D_\pi^- &\equiv D_u^{\pi^-} = D_{\bar{d}}^{\pi^+} = D_{\bar{u}}^{\pi^+} = D_{\bar{d}}^{\pi^-}, \\ D_s^\pi &\equiv D_s^{\pi^+} = D_{\bar{s}}^{\pi^-} = D_{\bar{u}}^{\pi^+} = D_{\bar{s}}^{\pi^+}. \end{aligned} \tag{46}$$

For the quark to kaon fragmentation functions, the following relations are valid under charge conjugation[?]:

$$\begin{aligned} D_K^+ &\equiv D_u^{K^+} = D_{\bar{u}}^{K^-} = D_{\bar{s}}^{K^+} = D_s^{K^-}, \\ D_K^- &\equiv D_u^{K^-} = D_{\bar{u}}^{K^+} = D_{\bar{s}}^{K^-} = D_s^{K^+}, \\ D_d^K &\equiv D_d^{K^+} = D_{\bar{d}}^{K^+} = D_{\bar{d}}^{K^-} = D_d^{K^-}. \end{aligned} \tag{47}$$

For this experiment, which covers $0.110 < x < 0.461$, we will assume a symmetrical strange quark distribution and polarization ($s(x) = \bar{s}(x)$, $\Delta s(x) = \Delta\bar{s}(x)$) and neglect heavy quark contributions.

B.1 Spin-dependent and spin-independent cross sections

According to Eq. 44, semi-inclusive π^+ and π^- cross section on proton and neutron are:

$$\begin{aligned} 9\sigma_p^{\pi^+} &= (4u + \bar{d})D_\pi^+ + (4\bar{u} + d)D_\pi^- + (s + \bar{s})D_s^\pi, \\ 9\sigma_p^{\pi^-} &= (4u + \bar{d})D_\pi^- + (4\bar{u} + d)D_\pi^+ + (s + \bar{s})D_s^\pi, \\ 9\sigma_n^{\pi^+} &= (4d + \bar{u})D_\pi^+ + (4\bar{d} + u)D_\pi^- + (s + \bar{s})D_s^\pi, \\ 9\sigma_n^{\pi^-} &= (4d + \bar{u})D_\pi^- + (4\bar{d} + u)D_\pi^+ + (s + \bar{s})D_s^\pi, \end{aligned} \tag{48}$$

the explicit x, z, Q^2 dependence has been left out to save space whenever not causing confusion. The semi-inclusive K^+ and K^- cross sections are:

$$9\sigma_p^{K^+} = (4u + \bar{s})D_K^+ + (4\bar{u} + s)D_K^- + (d + \bar{d})D_d^K,$$

$$
\begin{aligned}
9\sigma_p^{K^-} &= (4u+\bar{s})D_K^- + (4\bar{u}+s)D_K^+ + (d+\bar{d})D_d^K, \\
9\sigma_n^{K^+} &= (4d+\bar{s})D_K^+ + (4\bar{d}+s)D_K^- + (u+\bar{u})D_d^K, \\
9\sigma_n^{K^-} &= (4d+\bar{s})D_K^- + (4\bar{d}+s)D_K^+ + (u+\bar{u})D_d^K. \qquad (49)
\end{aligned}
$$

To get the spin-dependent cross sections ($\Delta\sigma^h$), one replaces the quark distributions in Eq. 48 and 49 with the quark polarization distributions.

B.2 The asymmetries expressed in "fixed-z purity"

The "fixed-z purity" is defined as the linear coefficients in front of Δq in the expression of double spin asymmetries, $A_1^h = \Delta\sigma^h/\sigma^h$. At the fixed value of z and x, these coefficients are obtained from the unpolarized parton distribution functions and the fragmentation function ratios. For example:

$$
A_{1p}^{\pi^+} = \frac{4\Delta u + \Delta\bar{d} + (4\Delta\bar{u} + \Delta d)\,\lambda_\pi + 2\Delta s\xi_\pi}{4u + \bar{d} + (4\bar{u} + d)\,\lambda_\pi + 2s\;\xi_\pi}, \qquad (50)
$$

$$
A_{1He}^{\pi^+} = \frac{4\Delta d + \Delta\bar{u} + \left(\Delta u + 4\Delta\bar{d}\right)\lambda_\pi + 2\Delta s\xi_\pi}{8u + 4d + \bar{u} + 2\bar{d} + \left(u + 2d + 8\bar{u} + 4\bar{d}\right)\lambda_\pi + 6s\xi_\pi}, \qquad (51)
$$

$$
A_{1p}^{K^+} = \frac{4\Delta u + \Delta s + (4\Delta\bar{u} + \Delta s)\,\lambda_K + (\Delta d + \Delta\bar{d})\xi_K}{4u + s + (4\bar{u} + s)\,\lambda_K + (d + \bar{d})\xi_K}, etc. \qquad (52)
$$

where the fragmentation function ratios are defined as:

$$
\begin{aligned}
\lambda_\pi(z) &= D_\pi^-(z)/D_\pi^+(z), \qquad & \xi_\pi(z) &= D_s^\pi(z)/D_\pi^+(z), \\
\lambda_K(z) &= D_K^-(z)/D_K^+(z), \qquad & \xi_K(z) &= D_d^K(z)/D_K^+(z). \qquad (53)
\end{aligned}
$$

C NLO global fit to DIS and SIDIS Data

The NLO global fit [11] to the existing DIS and SIDIS data are shown in Fig. 29.

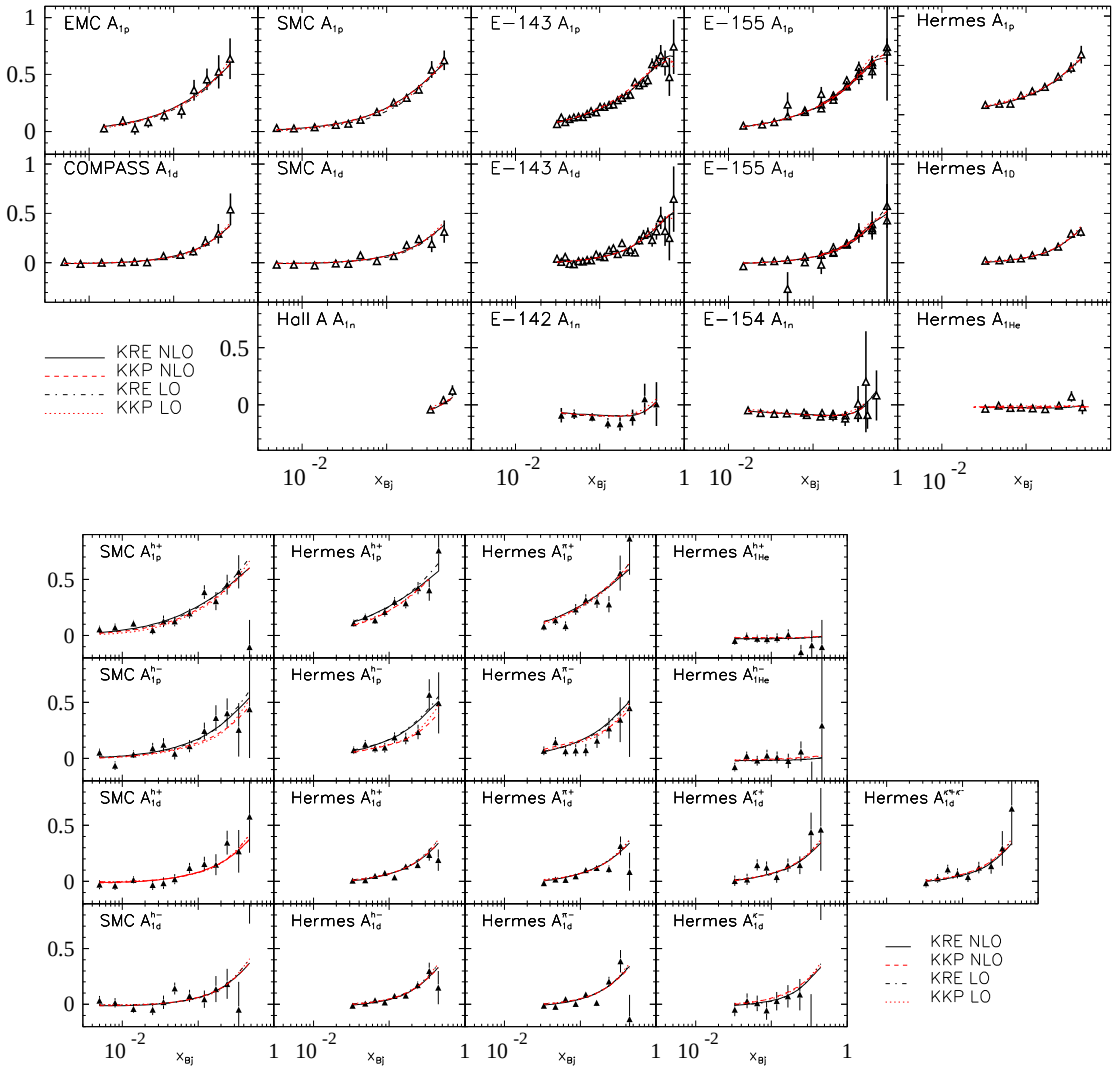

Figure 29: NLO global fit [11] to DIS data (top) and SIDIS data (bottom).

References

1. L. L. Frankfurt, M. I. Strikman, L. Mankiewicz, A. Schafer, E. Rondio, A. Sandacz and V. Papavassiliou, Phys. Lett. B **230**, 141 (1989); F. E. Close and R. G. Milner, Phys. Rev. D **44**, 3691 (1991). P. Mulders and R. D. Tangerman *Nucl. Phys.* B **461**, 197 (1996).
2. HERMES collaboration, *Phys. Rev. Lett.* **92**, 012005 (2004), and *Phys. Rev.* D **71**, 012003 (2005).
3. J. Wendland, Ph.D. Dissertation, Simon Fraser University, September (2003), and private communications, J. Wendland and A. Miller, June 2005.
4. The Spin Muon Collaboration, *Phys. Lett.* B **420**, 180 (1998).
5. The COMPASS Collaboration, *Phys. Lett.* B **660**, 458 (2008).
6. Xiangdong Ji, Jian-Ping Ma and Feng Yuan, hep-ph/0404183.
7. Xiangdong Ji, Jian-Ping Ma and Feng Yuan, hep-ph/0405085.
8. T. Navasardyan, et al. *Phys. Rev. Lett.* **98**, 022001 (2007).
9. E. Christova and E. Leader *Phys. Lett.* B **468**, 299 (1999) and *Nucl. Phys.* B **607**, 369 (2001).
10. D. de Florian and R. Sassot, *Phys. Rev.* D **62**, 094025 (2000), and D. de Florian, O. A. Sampayo and R. Sassot, *Phys. Rev.* D **57**, 5803 (1998)
11. D. de Florian, G. A. Navarro and R. Sassot, *Phys. Rev.* D **71**, 094018 (2005), and private communications (2005).
12. D. de Florian, R. Sassot, M. Stratmann and W. Vogelsang, *Phys. Rev. Lett.* **101**, 072001 (2008).
13. X. Jiang, G. A. Navarro and R. Sassot, *Eur. Phys. J.* C **47**, 81 (2006).
14. G. Bunce, N. Saito, J. Soffer and W. Vogelsang, Ann. Rev. Nucl. Part. Sci. **50**, 525 (2000).
15. Jefferson Lab Hall A, X. Zheng, *et al.*, *Phys. Rev. Lett.* **92**, 012004 (2004).
16. Jefferson Lab Hall A, K. Kramer *et al.*, nucl-ex/0506005.
17. Dressler, B. *et al.*, *Eur. Phys. J.* **C14**, 147 (2000).
18. F. G. Cao, A. I. Signal, *Eur. Phys. J.* C **21**, 105 (2001).
19. Glück, M. *et al.*, *Phys. Rev.* D **63**, 094005 (2001).
20. Blümlein, J., Böttcher, H., hep–ph/0203155, *Nucl. Phys. B*, (2002) in press.
21. HERMES collaboration, K. Ackerstaff *et al.*, *Phys. Lett.* B **464**, 123 (1999).
22. D. Graudenz, *Nucl. Phys.* B **432**, 351 (1994).
23. D. de Florian, C. A. Garcia Canal, R. Sassot, *Nucl. Phys.* B **470**, 195 (1996).
24. Marco Stratmann and Werner Vogelsang, *Phys. Rev.* D **64**, 114007 (2001)
25. A. N. Sissakian, O. Yu. Shevchenko and O. N. Ivanov, *Phys. Rev.* D **70**, 074032 (2004)
26. E. A. Hawker, *et al.*, *Phys. Rev. Lett.* **80**, 3715 (1998).
27. J. C. Peng, *et al.*, *Phys. Rev.* D **58**, 092004 (1998). *Eur. Phys. J.* **C5**, 461 (1998).
28. J.-C. Peng, *Eur. Phys. J.* A **18**, 395 (2003).
29. E. Eichten, I. Hinchliffe, C. Quigg, *Phys. Rev.* D **45**, 2269 (1992).

30. A. W. Thomas, *Phys. Lett.* B **126**, 97 (1983).
31. R. J. Fries, A. Schafer, *Phys. Lett.* B **443**, 40 (1998).
32. K. G. Boreskov, A. B. Kaidalov, *Eur. Phys. J.* C **10**, 143 (1999).
33. S. Kumano, M. Miyama, *Phys. Rev.* D **65**, 034012 (2002).
34. R. J. Fries, A. Schafer, C. Weiss, hep-ph/0204060.
35. M. Gluck *et al.*, *Phys. Rev.* D **63**, 094005 (2001).
36. F. M. Steffens, *Phys. Lett.* B **541**, 346 (2002).
37. B. Dressler *et al.*, hep-ph/9809487.
38. M. Wakamatsu, T. Watabe, *Phys. Rev.* D **62**, 017506 (2000).
39. A. Dorokhov, hep-ph/0112332.
40. C. Bourrely, J. Soffer and F. Buccella, *Eur. Phys. J.* C **23**, 487 (2002), and *Eur. Phys. J.* C **41**, 327 (2005).
41. R. S. Bhalerao, *Phys. Rev.* C **63**, 025208 (2001).
42. Jefferson Lab experiment E06-010, E. Cisbani, J.-P. Chen, H. Gao, X. Jiang and J.-C. Peng co-spokespersons.
43. T. Sloan, G. Smadja and R. Voss, *Phys Rep.* 162 (1988) 45.
44. P. Degtiarenko, private communications, 2007.
45. Lai, H.L. *et al.*, *Eur. Phys. J.* **C12**, 375 (2000).
46. B. A. Kniehl, G. Kramer, and B. Potter, *Nucl. Phys.* B **582**, 514 (2000).
47. D. Gaskell, private communication.
48. HERMES Collaboration preliminary results (http://www-hermes.desy.de)
49. P. Geiger, Ph.D. Dissertation, Ruprecht-Karls-University, Heidelberg (1998).
50. A. Nogga, Ph. D. thesis, Ruhr-Universität Bochum, Bochum, Germany (2001), p.72.
51. J.L. Friar *et al.*, Phys. Rev. C **42**, 2310 (1990).
52. C. Ciofi degli Atti *et al.*, Phys. Rev. C **48**, R968 (1993).
53. F. Bissey *et al.*, Phys. Rev. C **64**, 024004 (2001);
54. M. Sargsian, private communications, (2004).
55. S. Kretzer, *Phys. Rev.* D **62**, 054001 (2000).
56. J.M. Niczyporuk and E.E.W. Bruins, *Phys. Rev.* D **58**, 091501 (1998).
57. B. Anderson, G. Gustafson, G. Ingelmann, and T. Sjöstrand, *Phys. Rep.* **97**, 31 (1983).